The Plant Cell, Vol. 22: 4195–4215, December 2010, www.plantcell.org

Nucleocytoplasmic Distribution Is Required for Activation of Resistance by the Potato NB-LRR Receptor Rx1 and Is Balanced by Its Functional Domains [W]

Erik Slootweg,[a,1] Jan Roosien,[a] Laurentiu N. Spiridon,[b] Andrei-Jose Petrescu,[b] Wladimir Tameling,[c] Matthieu Joosten,[c] Rikus Pomp,[a] Casper van Schaik,[a] Robert Dees,[d] Jan Willem Borst,[e] Geert Smant,[a] Arjen Schots,[d] Jaap Bakker,[a,f] and Aska Goverse[a,f]

[a] Laboratory of Nematology, Department of Plant Sciences, Wageningen University, 6708 PB Wageningen, The Netherlands
[b] Institute of Biochemistry of the Romanian Academy, 060031 Bucharest, Romania
[c] Laboratory of Phytopathology, Department of Plant Sciences, Wageningen University, 6708 PB Wageningen, The Netherlands
[d] Laboratory of Molecular Recognition and Antibody Technology, Department of Plant Sciences, Wageningen University, 6708 PB Wageningen, The Netherlands
[e] Laboratory of Biochemistry, Department of Agrotechnology and Food Sciences, Wageningen University, 6703 HA Wageningen, The Netherlands
[f] Centre for BioSystems Genomics, 6700 AB Wageningen, The Netherlands

The Rx1 protein, as many resistance proteins of the nucleotide binding–leucine-rich repeat (NB-LRR) class, is predicted to be cytoplasmic because it lacks discernable nuclear targeting signals. Here, we demonstrate that Rx1, which confers extreme resistance to *Potato virus X*, is located both in the nucleus and cytoplasm. Manipulating the nucleocytoplasmic distribution of Rx1 or its elicitor revealed that Rx1 is activated in the cytoplasm and cannot be activated in the nucleus. The coiled coil (CC) domain was found to be required for accumulation of Rx1 in the nucleus, whereas the LRR domain promoted the localization in the cytoplasm. Analyses of structural subdomains of the CC domain revealed no autonomous signals responsible for active nuclear import. Fluorescence recovery after photobleaching and nuclear fractionation indicated that the CC domain binds transiently to large complexes in the nucleus. Disruption of the Rx1 resistance function and protein conformation by mutating the ATP binding phosphate binding loop in the NB domain, or by silencing the cochaperone *SGT1*, impaired the accumulation of Rx1 protein in the nucleus, while Rx1 versions lacking the LRR domain were not affected in this respect. Our results support a model in which interdomain interactions and folding states determine the nucleocytoplasmic distribution of Rx1.

INTRODUCTION

Disease resistance (R) proteins are the central actors in the cell-based innate immune system of plants. They are highly specific in the detection of certain pathogens and initiate an array of defense responses to prevent further spreading of the pathogen, often culminating in self-destruction of the attacked cell (Martin et al., 2003). In addition, other immune receptors, thought to represent a more ancient immune system, sense highly conserved pathogen-associated molecular patterns (PAMPs) (Navarro et al., 2004; Zipfel et al., 2004; Heese et al., 2007). Pathogen-specific R proteins may have evolved to recognize pathogen effectors that neutralize the weak PAMP-triggered immune responses (Jones and Dangl, 2006). R proteins sense the pathogen either by direct interaction with its effectors or indirectly by guarding host factors that are modified by pathogen effectors (Jia et al., 2000; de Wit, 2002; Deslandes et al., 2003; Jones and Takemoto, 2004; Dodds et al., 2006).

Members of the most abundant class of R proteins, the intracellular nucleotide binding–leucine-rich repeat (NB-LRR) proteins, consist of a C-terminal LRR recognition domain, a central nucleotide binding domain (NB-ARC), and at the N terminus often either a Toll-Interleukin Receptor-like (TIR) domain or a putative coiled coil (CC) domain. These N-terminal domains were originally thought to be the signaling adaptor modules, but only for TIR domains could such signaling function be shown (Swiderski et al., 2009). Recently, several N-terminal CC domains have been shown to interact with host proteins targeted by pathogen effectors and that act as guarded bait in an indirect or facilitated effector recognition (Collier and Moffett, 2009). The central NB-ARC domain likely functions as a conformational switch, and nucleotide binding and ATPase activities have been observed for R proteins (Tameling et al., 2002; Takken and Tameling, 2009). It is thought that R proteins exist in an ADP-bound resting state, which can change to an ATP-bound signaling-competent active state upon pathogen recognition.

Recent studies have placed the nucleus in the center of attention for plant disease resistance signaling. Several R proteins, including N, MLA, RPS4, and snc1, have been found in the

[1] Address correspondence to erik.slootweg@wur.nl.
The author responsible for distribution of materials integral to the findings presented in this article in accordance with the policy described in the Instructions for Authors (www.plantcell.org) is: Erik Slootweg (erik.slootweg@wur.nl).
[W] Online version contains Web-only data.
www.plantcell.org/cgi/doi/10.1105/tpc.110.077537

nucleus, and their nuclear localization is required for proper functioning (Burch-Smith et al., 2007; Shen et al., 2007; Wirthmueller et al., 2007; Cheng et al., 2009). The first R protein shown to have a nuclear localization was the *Arabidopsis thaliana* RRS1-R, which is a chimera of a TIR-NB-LRR protein and a WRKY-type transcription factor (Lahaye, 2002; Deslandes et al., 2003). RRS1-R interacts with its elicitor, the *Ralstonia solanacearum* effector PopP2 in the nucleus, and has been shown to cooperate with another nuclear R protein, RPS4, in resistance against multiple pathogens (Narusaka et al., 2009). According to the Rosetta stone principle (Eisenberg et al., 2000; Enright and Ouzounis, 2001), the existence of such a chimeric protein is an indication that in other instances an interaction with transcription factors is part of the R protein signaling mechanism. The discovery of the interaction between the barley (*Hordeum vulgare*) MLA proteins and the WRKY1 and WRKY2 transcription factors gave evidence that there is indeed a close link between R proteins and transcriptional regulation (Shen et al., 2007). In the presence of a *Blumeria graminis* effector, the R protein MLA10 interacts with the WRKY2 transcription factor in the nucleus. In the same study, WRKY1 and WRKY2 were shown to be suppressors of basal defense. MLA may activate the resistance response by lifting this suppression. The tobacco (*Nicotiana tabacum*) TIR-NB-LRR protein N, conferring resistance against *Tobacco mosaic virus*, also has a nuclear localization and associates with transcription factors via the LRR domain, whereas its N-terminal TIR domain indirectly binds the viral helicase p50 (Liu et al., 2004; Shen and Schulze-Lefert, 2007; Caplan et al., 2008a, 2008b). The finding that R proteins themselves are able to enter the nucleus indicates that the pathway between R protein activation and the downstream transcriptional reprogramming may contain fewer components than originally expected (Burch-Smith et al., 2007; Shen et al., 2007; Wirthmueller et al., 2007; Narusaka et al., 2009).

The underlying mechanism determining the distribution of R proteins between various subcellular compartments is not well understood. Large proteins like R proteins cannot diffuse freely from one compartment to another and need to pass through selective pores to enter membrane-enclosed organelles like the nucleus or the endoplasmic reticulum. Complex mechanisms have evolved to shuttle proteins between the cellular compartments. Trafficking between the cytoplasm and the nucleus is coordinated around the nuclear pore complexes via nuclear import and export receptors and the small GTPase Ran (Alber et al., 2007; Cook et al., 2007). The classical monopartite or bipartite nuclear localization signals (NLSs) are well defined and consist of short stretches of basic residues (three to six Lys/Arg) that interact with specific binding surfaces on the import receptor importin α, which in turn forms a heterodimer with importin β (Görlich and Kutay, 1999). Nuclear export is directed via Leu-rich nuclear export signals (NESs), which interact with the nuclear export receptor (exportin) (Haasen et al., 1999; Hutten and Kehlenbach, 2007). Several NB-LRR proteins, like RRS1-R, RPS4, and SNC1, do contain functional NLS sequences (Deslandes et al., 2003; Wirthmueller et al., 2007; Cheng et al., 2009). However, many R proteins of the NB-LRR class, including ones with a nuclear localization like N and MLA, lack a discernable localization signal, and as a result it was originally assumed that R proteins are localized in the cytoplasm.

The potato (*Solanum tuberosum*) Rx1 protein confers a highly efficient resistance to most *Potato virus X* (PVX) strains and has proven to be a valuable model for understanding R protein functioning. The resistance response it triggers after recognizing the viral coat protein (CP) is fast and under normal circumstances does not require the induction of cell death to stop virus replication (Bendahmane et al., 1999). The Rx1-induced response includes the specific inhibition of the translation of viral RNA via Argonaute-like proteins (Bhattacharjee et al., 2009). The subdomains of Rx1 cooperate via several intramolecular interactions. Recognition of the CP has been linked to a disruption of the interaction between the LRR and the CC-NB-ARC domains (Moffett et al., 2002; Rairdan et al., 2008). The MHD motif in the ARC2 domain, in which substitutions can lead to constitutive activity, is thought to act as a sensor integrating the recognition-mediated conformation changes and the nucleotide binding state of the protein. The interaction between the N-terminal half of the LRR and the bordering ARC2 subdomain needs to be well tuned as incompatibility between these domains can lead to constitutive activity, indicating that in the wild-type protein, their interaction has an autoinhibitory function (Rairdan and Moffett, 2006). Two studies independently showed that the CC domain interacts with a Ran GTPase Activating Protein (RanGAP2), a protein that plays a role in nucleocytoplasmic trafficking via the cytoplasm specific stimulation of RanGTPase activity (Sacco et al., 2007; Tameling and Baulcombe, 2007). Silencing of *RanGAP2* leads to a reduced Rx1-mediated resistance, whereas overexpression is associated with an increased Rx1 activity. However, its exact role in Rx1 signaling has not yet been elucidated.

Here, we describe the subcellular localization of Rx1 and the role the subcellular compartments play in Rx1 functioning. Furthermore, to understand the mechanisms behind the subcellular distribution of Rx1, we studied the contribution of the functional Rx1 subdomains to its localization. As with many R proteins of the NB-LRR family, a cytoplasmic localization of Rx1 is predicted because no classical linear NLSs can be found in the sequence and the size of the protein exceeds the limit for passive transport into the nucleus. However, fusions with fluorescent proteins showed that Rx1 is localized in both the cytoplasm and the nucleus. To investigate the effect on Rx functioning, both the CP elicitor and Rx1 were redirected to either compartment using exogenous targeting signals. Depletion of the elicitor from the cytoplasm by fusing it to a nuclear import signal showed that Rx1 needs to be activated in the cytoplasm and that the PVX CP is not able to activate Rx1 in the nucleus. Moreover, fusing a nuclear import or export signal to Rx1 demonstrated that both the nucleus and the cytoplasm are required for Rx1 functioning. Expression of individual Rx1 domains and deletion constructs as fluorescent protein fusions showed that the CC domain is predominantly localized in the nucleus and is required for the accumulation of full-length Rx1 protein in the nucleus. Further analysis of the CC secondary structure and various structure-based deletion constructs of the CC revealed no autonomous linear sequences responsible for nuclear translocation of the Rx1 protein. Photobleaching experiments and cell fractionation experiments revealed that the nuclear accumulation of the CC

appears to be caused by transient interactions with relatively immobile nuclear components and not by strong, active nuclear import signals. Furthermore, we demonstrate that disrupting the function and overall conformation of the Rx1 protein by mutating the ATP/ADP binding phosphate binding loop (P-loop), or by silencing the cochaperone *SGT1*, impaired the translocation of the full-length Rx1 protein to the nucleus, whereas Rx1 versions lacking the LRR domain were not affected. The interplay between the domains and the possible role of conformational changes in R protein signaling and localization are discussed.

RESULTS

Rx1 Is Located in Both the Cytoplasm and Nucleus

Rx1 is a 110-kD modular protein that, upon recognizing the CP of the plant virus PVX, mediates a strong local resistance response inhibiting the viral replication and systemic spreading. Based on size and the absence of transmembrane domains or specific subcellular targeting motifs in the amino acid sequence, Rx1 is assumed to be located in the cytoplasm. To test this assumption, we generated N- or C-terminal fluorescent protein (FP) fusions of Rx1 (Figure 1A). The green fluorescent protein (GFP)-fused versions were expressed by agroinfiltration in *Nicotiana benthamiana* leaves. Optimal fluorescence levels for microscopy imaging were reached after 2 to 3 d. Fluorescence was studied in living epidermal cells of the abaxial side of the leaf using confocal laser scanning microscopy. The GFP-fused Rx1 constructs accumulated to relatively low levels compared with free GFP, but stayed well above background fluorescence levels. With these microscope settings, no fluorescence in the GFP channel could be observed in cells transformed with an empty vector (Figure 1B). GFP fluorescence was observed in both the cytoplasm and the nucleus for GFP-Rx1 and for Rx1-GFP (Figure 1B). Detailed imaging of nuclei and surrounding cytoplasm in cells expressing GFP-Rx1 showed a slightly higher intensity in cytoplasm compared with the nucleus, whereas free GFP shows an equal intensity in cytoplasm and nucleus. Because the threshold for free diffusion to and from the nucleus is around 40 kD in plant cells (Merkle, 2003), we did not expect a nuclear localization for the fluorescent Rx1 proteins, which have a predicted mass of 140 kD. No breakdown products were detected after analyzing the expressed GFP-Rx1 by anti-GFP immunoblotting, excluding the possibility that the nuclear signal is derived from smaller GFP-containing peptides (Figure 1C).

To ensure that steric hindrance from the FP fusion did not interfere with R protein functionality, we tested the ability of FP-fused Rx1 to induce cell death and confer PVX resistance. The ability of GFP-Rx1 and Rx1-GFP to induce a PVX CP-specific hypersensitive response (HR) was tested by transient coexpression in *N. benthamiana* leaves with the avirulent (CP106) or virulent (CP105) CP or with GFP as a control for autoactivation. Expressed from the 35S promoter, both the N- and C-terminal GFP fusions of Rx1 gave a strong HR to the avirulent CP (CP106) (Figure 1D). A delayed and weaker HR was observed when the GFP-fused Rx1 constructs were coexpressed with the virulent CP (CP105) (Figure 1D). Apparently, the N- or C-terminal fusion of a fluorescent protein slightly broadens Rx1 recognition specificity or sensitizes Rx1 activation as Rx1 without GFP fusion does respond to CP105 under similar conditions. This response is not the effect of autoactivation as no cell death occurred after coexpression of the Rx1 constructs with GFP (Figure 1D). Recognition of the PVX CP by Rx1 was earlier shown to depend on the identity of two amino acid residues in the CP sequence (Querci et al., 1995), and a broadening of Rx1 recognition has been reported for Rx1 LRR mutants (Farnham and Baulcombe, 2006).

In addition, potato plants expressing cauliflower mosaic virus (CaMV) 35S promoter–driven yellow fluorescent protein (YFP)-Rx1 were fully resistant to the avirulent PVX_{UK3} but not to the PVX_{HB} breaker strain (Figure 1E). The extreme resistance phenotype was similar to that of the resistant potato clone SH, which contains Rx1 in its genetic background. The FP-fused Rx1 variants respond more sensitive to the virulent PVX CP when expressed from the 35S promoter but are further fully functional and confer a wild-type-like PVX resistance in stable potato transformants.

A Balanced Nucleocytoplasmic Distribution of Rx1 Is Required for Full Functionality

After finding that Rx1 resides in both the nuclear and cytoplasmic compartment of the cell, the first question that came to mind was if its presence in either compartment plays a role in the Rx1-mediated resistance and cell death response. Recent publications have shown that decreasing the nuclear concentration of R proteins like the barley R protein MLA10 or the tobacco protein N by adding an exogenous nuclear export signal strongly limits their ability to induce defense signaling (Burch-Smith et al., 2007; Shen et al., 2007).

To test if the subcellular distribution of Rx1 is of importance for its function, we created a set of constructs of the full Rx1 protein fused to either an NLS or NES. The addition of these targeting signals does not fully exclude the protein from either compartment, but enhances the active transport into (NLS) or out of the nucleus (NES) and is thereby expected to shift the balance between the nuclear and cytoplasmic pools of Rx1. To redirect Rx1 to the nucleus, the well-known SV40 Large T-antigen monopartite NLS was chosen (Lanford and Butel, 1984; Haasen et al., 1999). The PKI nuclear export signal (Wen et al., 1995) was applied to direct Rx1 from the nucleus to the cytoplasm. As controls, fusions were made with mutated versions of these targeting signals (nes* and nls*) (Figure 2A). Confocal microscopy imaging of the constructs expressed from the 35S promoter in *N. benthamiana* confirmed that the NES and NLS sequences were able to redirect the localization of the GFP-Rx1 constructs, whereas GFP-Rx1 constructs with a mutated version of the targeting signal had a localization pattern identical to the original GFP-Rx1 construct (Figure 2A).

When the NES or NLS versions of 35S:GFP-Rx1 were transiently coexpressed with the avirulent PVX:GFP amplicon or the elicitor CP106 in *N. benthamiana*, no change in virus spreading or the severity of the induced cell death response could be found between the versions with a functional or with a mutated targeting signal. However, this may be due to the fact that expression of Rx1 was controlled by the strong CaMV 35S promoter. Under these conditions, Rx1 is able to mediate a strong and fast

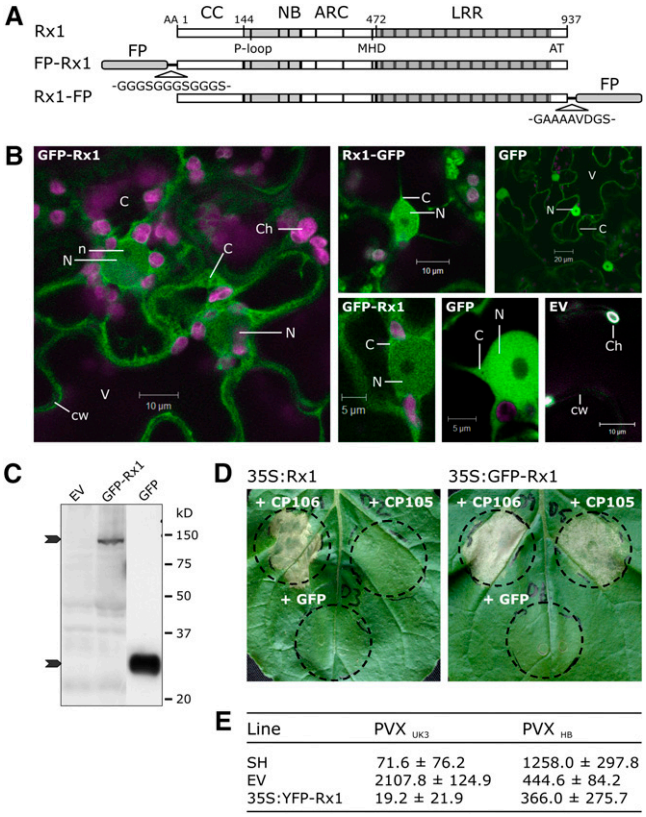

Figure 1. Subcellular Localization of the Full-Length Rx1 Protein.

(A) Schematic overview of the N- and C-terminal FP fusions of full-length Rx1. Both YFP (citrine YFP) and GFP (enhanced GFP) fusions were made. The amino acid sequences of the linkers connecting the FP to Rx1 are shown. Expression of the fusion constructs was controlled by the CaMV 35S promoter.

(B) Localization pattern of GFP-Rx1, Rx1-GFP, and GFP. The GFP-labeled proteins were imaged by confocal microscopy in epidermal cells of transiently transformed *N. benthamiana* leaves. Empty vector (EV) transformed cells are shown as controls for background fluorescence. Subcellular structures are indicated (C, cytoplasm; Ch, chloroplast; cw, cell wall; n, nucleolus; N, nucleus; V, vacuole). Images were taken 3 (GFP-Rx1, Rx1-GFP, and EV) and 2 (GFP) d after agroinfiltration. For GFP-Rx1 and GFP, a nucleus and the surrounding cytoplasm are shown in more detail.

(C) Immunoblot of protein extracts from *N. benthamiana* leaves transiently transformed with GFP-Rx1, an empty vector control (EV) or free GFP. Protein was detected with an anti-GFP antibody. The two arrows indicate the position of GFP-Rx1 (140 kD) and GFP (27 kD) on the blot. The GFP sample was diluted 1:10.

(D) Response of Rx1 or GFP-Rx1 when coexpressed with the avirulent PVX CP (CP106), the virulent PVX CP (CP105), or a negative control (GFP) in an agroinfiltration assay on *N. benthamiana* leaves. Images were taken 2 d after infiltration.

(E) Virus resistance assay with the avirulent PVX strain PVX UK3 and the virulent strain PVX HB. The susceptible potato genotype line V was transformed with either an empty pBINPLUS expression cassette (EV) or 35S:YFP-Rx1. The potato genotype SH containing Rx1 in its genomic background was used as a positive control. Per treatment, three plants from three independent primary transformants were assayed. Virus concentrations were measured at 21 d after inoculation in an ELISA with a PVX-specific antibody (mean absorbance values at A_{405} [±SD]).

resistance response, and we often observed cell death within 30 h after agroinfiltration. Therefore, it is anticipated that the strength of the response makes it difficult to distinguish more subtle changes in functionality.

To make the Rx1 resistance assays more sensitive, we decided to reduce the protein levels of Rx1 by lowering the translational efficiency of the Rx1 construct. An out-of-frame second start codon was introduced just upstream of the original start codon, resulting in a 5 to 10 times reduction of the Rx1 protein levels (Figure 2B) (Kozak, 1995, 1999). Rx1-GFP expressed from this so-called leaky scan ($35S_{LS}$) promoter can still induce a PVX CP-dependent HR. However, no phenotypic differences in the strength of HR could be observed upon targeting of Rx1 to either the nucleus or cytoplasm.

To exclude the possibility that phenotypic differences were still masked due to overexpression of the PVX elicitor, the Rx1 constructs were coexpressed with a PVX:GFP amplicon in *N. benthamiana* leaves (Peart et al., 2002a). Virus resistance could then be monitored by visualizing the spread of GFP expression from the amplicon or by an ELISA assay with antibodies directed against the viral CP. In this virus resistance assay, the NES version of Rx1-GFP ($35S_{LS}$:Rx1-GFP-NES-8HA) allowed more PVX:GFP to spread than the version with the mutated targeting signal (nes) as visualized by a higher number of HR foci and the detection of higher levels of GFP fluorescence under illumination by UV light (Figure 2C). Consistently higher levels (65% ± 60%) of virus were detected by anti-PVX ELISA assays in the samples where Rx1 was fused to a functional NES in comparison to the nes* samples (33 sample pairs, paired *t* test, one-tail $P = 3 \times 10^{-7}$) (Figure 2D). Redirecting Rx1 to the nucleus ($35S_{LS}$:Rx1-GFP-NLS-8HA) resulted in an even stronger reduction of resistance as seen when the virus accumulation was compared after coexpression of the PVX:GFP amplicon with the NLS- and mutated nls*-tagged Rx1 versions. Higher PVX expressed GFP levels were clearly visible under UV light (Figure 2C), and 4 times more PVX CP was detected in the anti-PVX ELISA (Figure 2D) (11 sample pairs, paired *t* test, one-tail $P = 1 \times 10^{-4}$). The constructs with the mutated targeting signals (nes and nls) did not differ markedly from each other in their ability to stop PVX spreading and were indistinguishable from a similar Rx1 construct lacking any targeting sequence ($35S_{LS}$:Rx1-GFP) (data not shown). Furthermore, we could show on anti-HA/GFP immunoblots of whole-cell protein extracts that the Rx1 constructs with functional or nonfunctional mutated targeting signals accumulate to similar levels in the cell (Figure 2E).

In conclusion, the Rx1 pools in both nuclear and cytoplasmic compartments of the cell appear to play a role in the functioning of Rx1, but in contrast with what was reported for several other R proteins, it seems that shifting the Rx1 distribution to the cytoplasm has a relatively small effect on its functionality, whereas a stronger reduction in resistance is observed when most Rx1 is shifted to the nucleus.

Elicitor-Dependent Activation of Rx1 Occurs in the Cytoplasm

The path from R protein–mediated pathogen recognition to the resulting resistance response and cell death can be dissected in

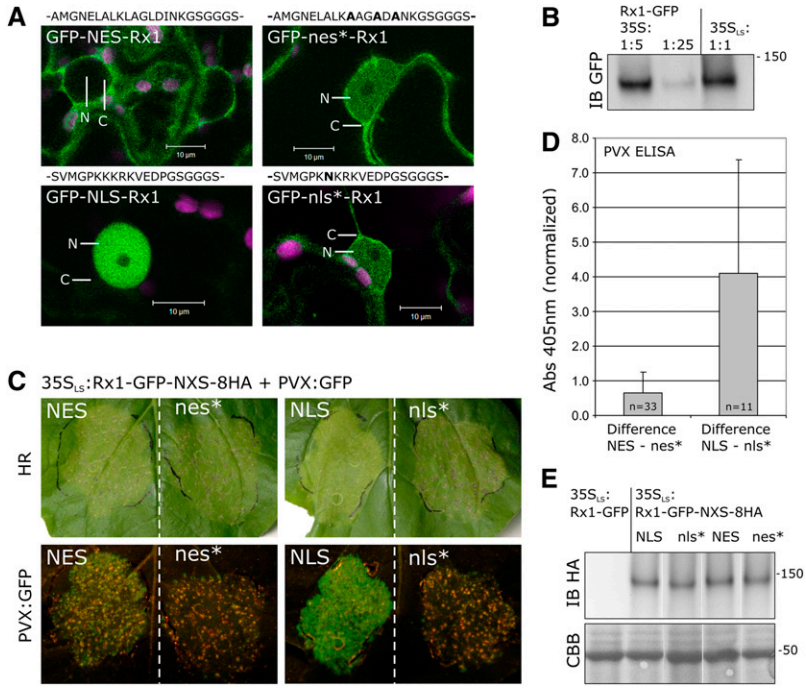

Figure 2. Modifying the Rx1 Localization by Exogenous Subcellular Targeting Signals.

(A) Redirecting Rx1 by the fusion of an NES or NLS. As control, both the NLS and NES mutated versions were used (nls* and nes*). The sequence of each targeting signal is depicted above the confocal microscopy image showing the localization of the construct in *N. benthamiana* cells. GFP fluorescence is shown in green and chlorophyll in magenta. Nucleus and cytoplasm surrounding it are indicated by N and C.

(B) The expression level of Rx1-GFP under control of the 35S and the $35S_{LS}$ (leaky scan) promoter compared by anti-GFP immunoblotting. The 35S:Rx1-GFP sample was diluted 5 and 25 times. The $35S_{LS}$:Rx1-GFP sample was not diluted.

(C) Transient resistance assay comparing the PVX resistance mediated by nuclear (NLS) or cytoplasmic (NES) targeted Rx1 under control of the $35S_{LS}$ promoter. Identical constructs with mutated targeting signals served as reference. Spreading of PVX:GFP from the coexpressed PVX amplicon can be seen by the number and size of the HR foci (top panels) or visualized by the fluoresence from the PVX-expressed GFP (bottom panels).

(D) PVX resistance mediated by the four $35S_{LS}$:Rx1-GFP-NXS-8HA variants analyzed by an anti-PVX CP ELISA. The Rx1 targeting variants were coexpressed with the avirulent PVX:GFP. The ELISA signal was normalized and the absorbance difference between NES and nes* or between NLS and nls* Rx1 samples was determined per leaf. The average signal differences and SD are shown.

(E) The stability of the four $35S_{LS}$:Rx1-GFP-NXS-8HA constructs was assessed by extracting the transiently expressed protein from *N. benthamiana* leaves and detecting it on an anti-HA immunoblot. The protein was extracted in 8 M urea and 100 mM DTT to ensure that all protein, including the nuclear fraction, could be detected.

multiple steps. By directing Rx1 to the nuclear or cytoplasmic compartment and observing the effect on the outcome of the reaction, it is not possible to conclude which step in the activation pathway is localization dependent. To differentiate the importance of the cytoplasm and the nucleus in the recognition step of the Rx1 activation pathway, we manipulated the nucleocytoplasmic distribution of the avirulent PVX CP.

Fluorescent versions of avirulent (CP106) and virulent (CP105) PVX CPs were constructed by fusing a fluorescent protein (cyan fluorescent protein [CFP] or GFP) to the N terminus of the CPs. The fluorescent fusions did not alter the Rx1-mediated recognition (see Supplemental Figure 1 online) and have been shown not to hamper the functioning of the CP in the formation of viral particles (Santa Cruz et al., 1996).

Confocal microscopy showed that the avirulent and virulent CPs do not differ in their subcellular distribution in *N. benthamiana* leaf epidermis cells (Figure 3A). Both were found in the nucleus and the cytoplasm in equal intensities, as was expected because the mass of the fusion products (~45 kD) does not exceed the size exclusion limit of the nuclear pore and their sequence does not contain specific targeting signals (Figure 3A). These observations are in accordance with the localization pattern described earlier (Batten et al., 2003).

To distinguish the role of the cytoplasm and nucleus in the recognition of PVX, we constructed versions of the CP that contained the SV40 NLS (Lanford and Butel, 1984; Haasen et al., 1999) or the PKI NES (Wen et al., 1995) and mutated versions of these signals as described previously for the Rx1 NES and NLS constructs. The NLS versions of the virulent and avirulent CPs are efficiently targeted to the nucleus, and the NES versions are almost completely excluded from the nucleus (Figure 3A). All NLS and NES versions are stable and expressed at similar levels, as was shown by immunoblotting (Figure 3B).

The ability of these CP versions to activate Rx1 was tested in agroinfiltration assays on *N. benthamiana* leaves. Transiently expressed Rx1 under control of the CaMV 35S promoter and

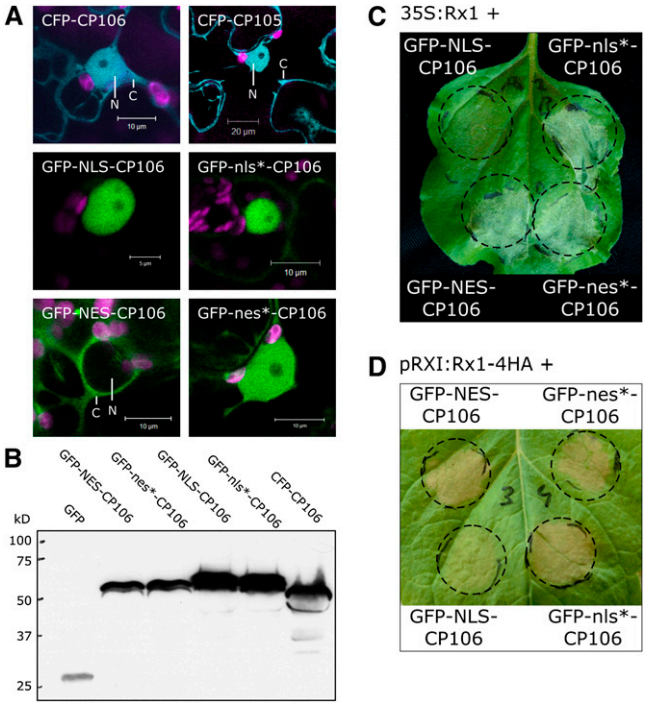

Figure 3. Nuclear-Targeted PVX CP Does Not Induce the Rx1 HR Response.

(A) Confocal image of the subcellular localization of the PVX CP when expressed as a fusion to CFP is shown in the top two panels (CFP-CP106, left; CFP-CP105, right) (CFP fluorescence, blue; chloroplast fluorescence, magenta). The localization of GFP-tagged versions of CP106 with a targeting signal (SV40 NLS, PKI NES, and mutated variants thereof) are shown in the bottom four panels. Detailed views of the nuclei are shown to display the fluorescence intensities in the cytoplasm (C) and nucleus (N) clearly.

(B) Anti-GFP immunoblot showing the protein levels of the targeted versions of the PVX CP in *N. benthamiana* leaf protein extracts.

(C) Response induced by exogenous targeted 35S:GFP-CP106 constructs coexpressed with 35S:Rx1. GFP-NLS-CP106 (SV40 NLS, PKKKRKVEDP), GFP-NES-CP106 (PK1 NES, NELALKLAGLDINK), and the mutated versions thereof (GFP-nls*-CP106, PKNKRKVEDP; GFP-nes*-CP106, NELALKAAGADANK) were coexpressed with 35S:Rx1 in an agroinfiltration assay in *N. benthamiana* leaves. At 2 d after infiltration, a clear HR was observed for all combinations except for the coexpression of Rx1 with GFP-NLS-CP106. The image was taken 3 d after infiltration.

(D) Response induced by exogenous targeted 35S:GFP-CP106 constructs transiently expressed in transgenic *N. benthamiana* expressing Rx1-4HA from its endogenous regulatory sequences.

Rx1-4HA stably expressed from its endogenous regulatory sequences in transgenic *N. benthamiana* plants were both tested for their response to the redirected PVX CP versions. All avirulent CP constructs elicited an HR within 2 d after the infiltration, except the construct containing the functional NLS (Figures 3C and 3D). The mutated NLS control construct (nls*) differs in only one amino acid (KKKRK > KNKRK) from the functional NLS construct, but can still fully elicit an Rx1-mediated HR.

From these results, we conclude that recognition of the PVX CP takes place in the cytoplasm and the nucleus does not provide an environment in which Rx1 can be activated. Our data also show that Rx1-mediated signaling requires no, or at least no high concentrations of, PVX CP in the nucleus, as no effect was observed upon adding a nuclear export signal to the avirulent CP.

The CC Domain Accumulates in the Nucleus and Is Required for Nuclear Localization of the Rx1 Protein

Rx1 cannot be excluded from either the nucleus or the cytoplasm without some loss of function, and the PVX CP can only activate Rx1 in the cytoplasm. However, it is not evident how Rx1 is balanced between the nuclear and cytoplasmic pools. No classical NLSs, which could explain for its presence in the nucleus, are predicted in the linear amino acid sequence of Rx1 (PredictNLS; Cokol et al., 2000). To gain insight in the mechanism underlying the observed nucleocytoplasmic distribution, we constructed a series of fluorescent domain deletion constructs of Rx1 (Figure 4A).

The Rx1 protein is composed of several flexibly linked domains, an N-terminal CC, an extended nucleotide binding domain (NB-ARC), and a C-terminal LRR domain. Upon coexpression as separate modules, these domains can interact and reconstitute a functional Rx1 protein (Moffett et al., 2002). This characteristic allowed us to test whether the fluorescent domain fusion constructs retained their ability to confer PVX resistance when coexpressed with the complementary parts of Rx1. The complementary combinations of the Rx1 domains were coexpressed with PVX:GFP, and the virus accumulation was assessed via an anti-PVX ELISA (Figure 4B). The N-terminal half of the Rx1 protein (CC-NB-ARC) proved to be sensitive to the position of the fluorescent fusion protein. The YFP-CC-NB-ARC product lost the ability to confer PVX resistance when expressed in trans with the LRR, even though the full-length Rx1 tolerates an N-terminal fluorescent protein fusion. CC-NB-ARC-GFP, on the other hand, could confer resistance in a complementation assay. In addition, the N-terminal fusion construct GFP-LRR was shown to be functional, and also for the CC-GFP, a wild-type-like PVX resistance was observed when coexpressed with the NB-ARC-LRR-GFP. Even the combination of the CC-GFP, NB-ARC-GFP, and GFP-LRR constructs in trans conferred an intermediate PVX resistance (Figure 4B). Apparently, when the fluorescent proteins are introduced at the positions where the full-length protein domains are linked, the assembly of the domains into a functional protein is not disrupted.

Confocal microscopy showed that the subcellular localization patterns of various fluorescent versions of Rx1 differed markedly from the full Rx1 protein (Figure 4C). Average nucleocytoplasmic distribution ratios were determined by comparing the fluorescence intensities in the nucleus and cytoplasm from the confocal images made under identical confocal settings (Figure 4D). In this way, it is possible to get an indication of the consistency of the subcellular distribution by comparing multiple cells. Higher values for I_N/I_C indicate a more nuclear localization, whereas higher values for I_C/I_N indicate a more cytoplasmic localization.

The CC-GFP (42 kD) construct showed markedly higher fluorescence intensities in the nucleus than in cytoplasm, something

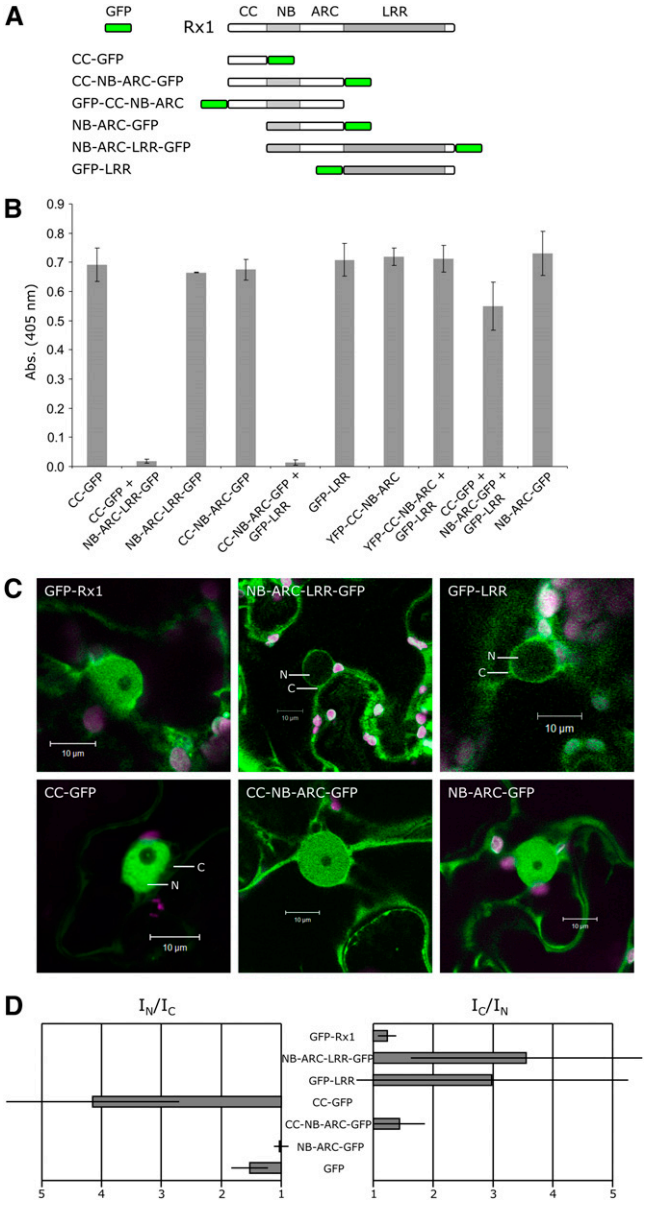

Figure 4. Subcellular Localization of Truncated Rx1 and Its Separate Domains.

(A) Schematic overview of the N- and C-terminal GFP fusions of the Rx1 subdomains and deletion constructs.

(B) Complementation in trans of the fluorescent constructs by the corresponding Rx1 domains in a transient virus resistance assay. Fluorescent fusions of the Rx1 subdomains were coexpressed with their complementary parts and avirulent PVX:GFP. Resistance was assessed via an anti-PVX ELISA 5 d after agroinfiltration. The average absorption at 405 nm (±SD) for four replicates is shown.

(C) Subcellular localization of the GFP-labeled truncated Rx1 polypeptides and separate domains shown by confocal imaging. Full-length GFP-Rx1 is shown for comparison. Images were taken 2 d after infiltration. Where fluorescent intensities strongly differ between cytoplasm (C) and nucleus (N) these compartments is indicated.

(D) Nucleocytoplasmic distribution of the fluorescent fusion proteins shown as fluorescent intensity ratios: nuclear intensity (I_N) divided by cytoplasmic intensity (I_C) and vice versa (I_C/I_N). Average fluorescence intensity ratios (±SD) were determined from the fluorescence intensities on the cytoplasm and nucleus in confocal images of eight *N. benthamiana* leaf epidermal cells with the Java application ImageJ.

that was not observed for the smaller GFP control (27 kD) or any of the other Rx1 domain constructs. CC-NB-ARC-GFP (80 kD) and NB-ARC-GFP (64 kD) showed an almost equal distribution between cytoplasm and nucleus, as observed for the full-length Rx1 protein. However, the NB-ARC-LRR-GFP (125 kD) construct was predominantly localized in the cytoplasm, indicating that the CC domain is directly or indirectly required for nuclear accumulation of the full Rx1. The high nuclear accumulation of the CC domain supported this interpretation. The LRR domain seemed to have an opposite role. The GFP-LRR protein was excluded from the nucleus (Figures 4C and 4D). Although Leu-rich NES motifs are predicted for the LRR (NetNES 1.1; la Cour et al., 2004), they overlap with the structural hydrophobic residues of the LRR repeat, which are not surface exposed (Kobe and Kajava, 2001). Therefore, it is not likely that this motif acts as a targeting signal. When fused to a triple GFP construct containing a weak NLS, the LRR fragment containing the putative NES did not show any NES activity; therefore, we assume that other factors than this motif determine the cytoplasmic localization of the LRR.

Nuclear Localization of Rx1 Requires a Nucleotide-Bound Conformation

The nucleotide bound to the NB and ARC domains acts as an anchor point determining the overall conformation of the Rx1 protein. It is hypothesized that the conformational change from an inactive to an active state involves changes in nucleotide binding status (Tameling et al., 2002, 2006) and intramolecular interactions (Moffett et al., 2002; Rairdan and Moffett, 2006; Rairdan et al., 2008). Mutations in the P-loop of the NB domain abolish the activity of Rx1 and disrupt the interaction between the CC domain and the NB-ARC-LRR but not between CC-NB-ARC and LRR (Moffett et al., 2002; Rairdan et al., 2008).

The mutation K176R was made in the Rx1 P-loop to study if the absence of a bound nucleotide would influence the Rx1 subcellular distribution. This mutation inactivated the protein completely. Analysis of the transiently expressed protein by immunoblots showed that the K176R mutant and the wild-type version of GFP-Rx1 accumulated to similar levels (Figure 5C). The fluorescence intensity of the GFP-Rx1 K176R construct was similar to the intensity measured for the GFP-Rx1 construct under identical microscope settings (Figure 5A). In contrast with wild-type GFP-Rx1, GFP-Rx1 K176R was almost absent from the nuclei (Figure 5A), which could be seen by the increase in the fluorescence intensity ratio between cytoplasm and nucleus (I_C/I_N) (Figure 5B).

Since in the localization study of the domain deletion constructs (Figure 4) higher I_C/I_N ratios seemed to be correlated with the presence of the LRR, we decided to introduce the P-loop

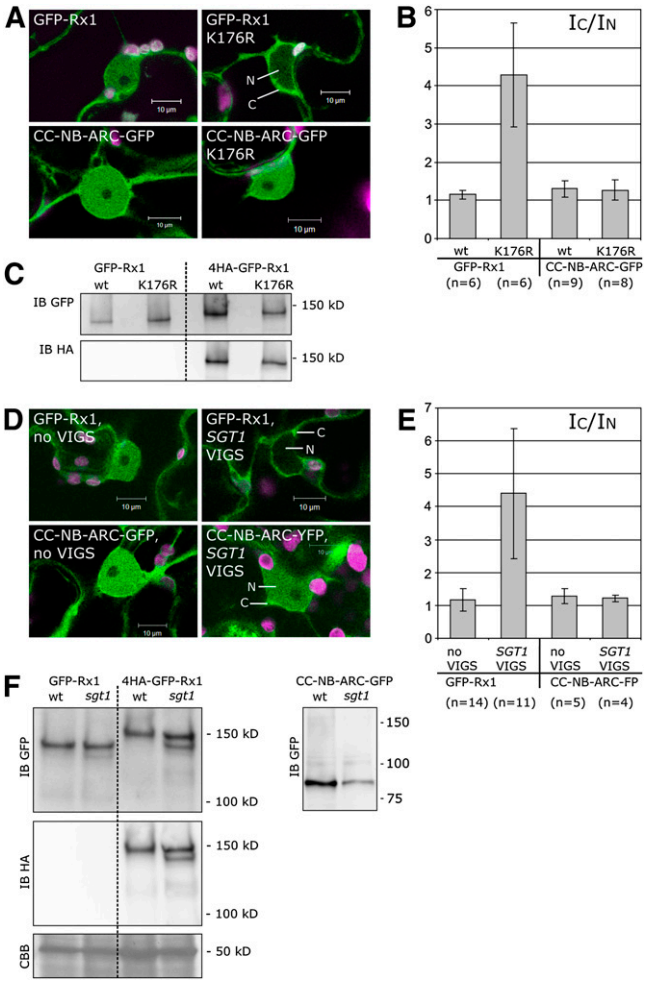

Figure 5. The Effect of the P-Loop Mutation K176R and *SGT1* Silencing on the Nucleocytoplasmic Distribution of Rx1.

(A) Confocal images of the subcellular localization of GFP-Rx1, GFP-Rx1 K176R (P-loop), CC-NB-ARC-GFP, and CC-NB-ARC-GFP K176R in *N. benthamiana* cells. Lower fluorescence levels can be seen for GFP-Rx1 K176R in the nucleus (N). The CC-NB-ARC-GFP K176R construct does not show a shift toward the cytoplasm (C).

(B) The average fluorescence intensity ratio between the cytoplasm (I_C) and the nucleus (I_N) was determined for 10 *N. benthamiana* cells per constructs. A higher ratio indicates fluorescence levels in the cytoplasm higher than in the nucleus. wt, wild type.

(C) HA and GFP immunoblot (IB) showing the accumulation levels of the wild-type and K176R versions of GFP-Rx1 and 4HA-GFP-Rx1.

(D) Confocal images of the subcellular localization of GFP-Rx1 and CC-NB-ARC-GFP expressed in wild-type or *SGT1*-silenced *N. benthamiana* leaves.

(E) GFP-Rx1 and Rx1 CC-NB-ARC-GFP were expressed in wild-type *N. benthamiana* and in *SGT1*-silenced *N. benthamiana*. The average intensity ratios (±SD) were determined for 10 cells per combination (I_C/I_N). A shift toward a more cytoplasmic localization of GFP-Rx1 in *SGT1*-silenced plants is seen as a higher average I_C/I_N. No such shift was observed for CC-NB-ARC-GFP.

(F) GFP and HA immunoblot on protein extracts from wild-type and *SGT1*-silenced *N. benthamiana* plants transiently expressing 35S:GFP-Rx1, 35S:4HA-GFP-Rx1, or 35S:CC-NB-ARC-GFP.

mutation in a construct lacking the LRR. Wild-type CC-NB-ARC-GFP was used for comparison. When expressed in *N. benthamiana* cells, the localization patterns of the wild type and of the K176R version of the CC-NB-ARC-GFP were indistinguishable (Figure 5A). CC-NB-ARC-GFP K176R was not excluded from the nucleus. Hence, we conclude that the nuclear exclusion of the full-length GFP-Rx1 K176R depends on the presence of the LRR domain.

Nuclear Localization of Rx1 Is Impaired upon Silencing of *SGT1*

SGT1 is known to be essential for the functioning of many R proteins, likely as part of an essential chaperone complex for R proteins (Austin et al., 2002; Azevedo et al., 2002, 2006; Botër et al., 2007). SGT1 has been found in the cytoplasm and also in the nucleus (Noël et al., 2007) and interacts with chaperones that have been implicated in assisting nuclear shuttling, like HSP90 or HSC70 (Tago et al., 2004; Kose et al., 2005; Brkljacic et al., 2009; Cazalé et al., 2009). We tested whether the absence of SGT1 would affect the localization of Rx1. *SGT1* expression was knocked down by TRV-based virus-induced gene silencing in *N. benthamiana* (Lu et al., 2003). The *SGT1*-silenced plants showed a clear change in morphology, as reported earlier (Peart et al., 2002b).

As expected, Rx1 coexpressed with the PVX CP could no longer induce an HR in *SGT1*-silenced plants (see Supplemental Figure 2 online). Protein levels of transiently expressed full-length GFP-Rx1, 4HA-GFP-Rx1, and the truncated CC-NB-ARC-GFP from wild-type and *SGT1*-silenced plants were analyzed by immunoblotting. Protein levels of GFP-Rx1 and 4HA-GFP-Rx1 were slightly reduced in the *SGT1*-silenced plants in which their localization was imaged. A small reduction was seen for CC-NB-ARC-GFP (Figure 5F). The subcellular localizations of GFP-Rx1 and CC-NB-ARC-GFP were studied using microscopic settings identical to those used for visualizing the subcellular localization in nonsilenced plants, which means that in the cells in which the protein was imaged, proteins levels were not markedly reduced.

The subcellular localization of the fluorescent Rx1 protein was clearly affected in *SGT1*-silenced plants (Figure 5D). In contrast with wild-type plants, the GFP-Rx1 fluorescence observed in the cells of *SGT1*-silenced plants was mostly excluded from the nucleus (Figures 5D and 5E). The CC-NB-ARC-GFP constructs lacking the LRR did not exhibit a shift toward the cytoplasm in the absence of SGT1. This suggests that the effect of SGT1 on the subcellular distribution of Rx1 is linked to its LRR domain. The empty vector control did not affect Rx1 distribution, excluding the possibility that the phenotype was a side effect of the silencing system. In the case of *SGT1* silencing, there is a reduction in total Rx1 levels when the silencing progresses (>5 weeks after TRV infection). However, these plants also exhibited lower fluorescence levels and were not used for imaging.

A Short Helix-Rich Segment Determines Nuclear Accumulation of the Rx1 CC Domain

The fact that the CC-GFP construct accumulated to higher levels in the nucleus than free GFP made it an interesting subject for

further investigation. Not much is known about the structural properties of R protein CC domains except that a conserved motif (-EDMVD- in Rx1) plays a role in the CC/NB-ARC-LRR interaction (Rairdan et al., 2008). To investigate whether a distinct sequence within the CC domain determines the nuclear localization of Rx1, we decided to create a set of GFP-fused sub-CC fragments based on the predicted secondary structure of the CC.

Boundaries of the CC domain were delineated with CDART, Interpro, and predictors for secondary structure and intradomain loop sequences. Both CDART and Interpro indicated that the NB-ARC domain starts at amino acid 136, while the helix propensity in Rx1 stops at around amino acid 115, as shown by the consensus secondary structure prediction. In addition, the Domain Linker Predictor indicated a high propensity for intradomain loop sequences between amino acids 115 and 135. All these data suggested that in Rx1 the CC domain can be set approximately between amino acids 1 and 115, in accordance with earlier in trans complementation assays of CC deletion constructs (Rairdan et al., 2008).

The consensus secondary structure profile indicates the presence of four major helical regions (H1, amino acids 2 to 20; H2, amino acids 25 to 45; H3, amino acids 51 to 69; H4, amino acids 76 to 115) joined by three loops that also showed a high propensity for intrinsic disorder (Figure 6A). In addition, more specialized predictors, such as SOPMA 5-state and BETATURN, indicated a high propensity for a β-turn between H2 and H3 (amino acids 45 to 50) and to a lesser extent between H3 and H4 (amino acids 73 to 77) (Figure 6A).

The four regions predicted to form helices were each fused to GFP, individually or in combination with neighboring helices, resulting in seven constructs (Figure 6B). All CC fragment constructs were shown to be stable by immunoblots with anti-GFP antibody (see Supplemental Figure 3 online). The subcellular distribution of five of these constructs was similar to free GFP, with an almost equal intensity in the cytoplasm and the nucleus (Figures 6C and 6D). However, two constructs, Rx1(1-45)-GFP and Rx1(45-116)-GFP, displayed a strikingly different distribution. Rx1(1-45)-GFP, containing the two predicted N-terminal helices (H1 and H2), was almost completely absent from the nucleus and predominantly present in the cytoplasm, despite its small size (32 kD). Rx1(1-45)-GFP showed an association with subcellular structures resembling Golgi bodies and the endoplasmic reticulum (Figure 6C). This subcellular localization pattern was not observed for fragments Rx1(1-20)-GFP (H1) or Rx1 (16-45)-GFP (H2), indicating that the combination of the two helices is essential for the cytoplasmic targeting of Rx1(1-45)-GFP. Rx1(45-116)-GFP (35 kD), containing the third and fourth predicted helixes (H3 and H4), had a strong nuclear accumulation, comparable with the full CC domain [Rx1(1-144)-GFP]. No such nuclear accumulation was observed for the overlapping fragments Rx1(45-87)-GFP (H3) or Rx1(79-116)-GFP (H4), showing that the combination of these two helices is required for the nuclear accumulation of Rx1(45-116)-GFP (Figures 6B and 6C).

To test if the CC fragments Rx1(1-45)-GFP and Rx1(45-116)-GFP could complement each other to form a functional CC, they were coexpressed with NB-ARC-LRR-GFP and avirulent PVX CP (CP106), either individually or in combination. Only when Rx1(1-45)-GFP, Rx1(45-116)-GFP, NB-ARC-LRR-GFP, and CP106 were combined did an HR occur, showing that both fragments are needed to reconstitute the ability of Rx1 to initiate a cell death response (Figure 6E). A similar complementation assay was used to determine if PVX resistance could be reconstituted (Figure 6F). Only when NB-ARC-LRR-GFP was combined with Rx1(1-45)-GFP and Rx1(45-116)-GFP was the spreading of PVX:GFP effectively blocked. These results demonstrate that the CC domain includes two nonoverlapping subdomains, each consisting of two α-helices, which show distinct localization patterns if expressed individually. The fragment containing helixes 3 and 4, however, seems to determine the nuclear accumulation observed for the full CC.

The CC Domain Is Sequestered in the Nucleus by Binding to Large Complexes

The CC constructs described in Figure 6 are all fusions with a single GFP, and none of the fusion products have a molecular mass >45 kD, leaving the question open whether the observed nuclear accumulation of the full CC-GFP and Rx1(45-116)-GFP resulted from active nuclear import via a transferable targeting signal or passive import through diffusion.

To limit the passive diffusion through the nuclear pore, GFP-β-glucuronidase (GUS) fusions were constructed for the CC domain [Rx1(1-144)] and for Rx1(45-116), which increased the overall mass of the constructs by ~70 kD (Figure 7B). As control, a GFP-GUS construct without targeting signals was made. The lack of fluorescence in the nucleus and the fluorescence that can be observed in the layer of cytoplasm surrounding the nucleus demonstrates that the nucleocytoplasmic distributions of the CC-GFP-GUS, Rx1(45-116)-GFP-GUS, and GFP-GUS proteins all shifted to an almost completely cytoplasmic localization compared with the single GFP constructs (Figure 7A). Coexpression of Rx1(45-116)-GFP-GUS with the interacting N-terminal WPP domain of RanGAP2 fused to an NLS (Rg2-ΔC-mC-NLS) restored the nuclear localization (Figure 7C). The GFP-GUS construct, which does not interact with RanGAP2, does not show this Rg2-ΔC-mC-NLS–induced relocalization (Figure 7C).

The nucleocytoplasmic distribution patterns of CC-GFP-GUS and Rx1(45-116)-GFP-GUS indicate that these sequences do not contain strong autonomous NLSs. A possible explanation for the nuclear accumulation of the Rx1 CC and fragment Rx1(45-116) in the nucleus in the absence of a NLS could be a combination of passive introduction into the nucleus combined with sequestering in the nucleus, partially preventing the transport back to the cytoplasm. If the Rx1 CC is held in the nucleus via an interaction, then one would predict that this would affect its diffusional freedom in the nucleus.

To test this hypothesis, local photobleaching was applied to the fluorescent fusion proteins, and the dynamics of fluorescence recovery were studied using fluorescence recovery after photobleaching (FRAP), a technique commonly used to study the diffusional behavior of nuclear proteins (Carrero et al., 2003; McNally, 2008). A small area in the nucleus was bleached, and fluorescence recovery was monitored. Subsequently, the recovery half-times were used to calculate the effective diffusion coefficients. Free GFP is known to diffuse unrestrictedly in the

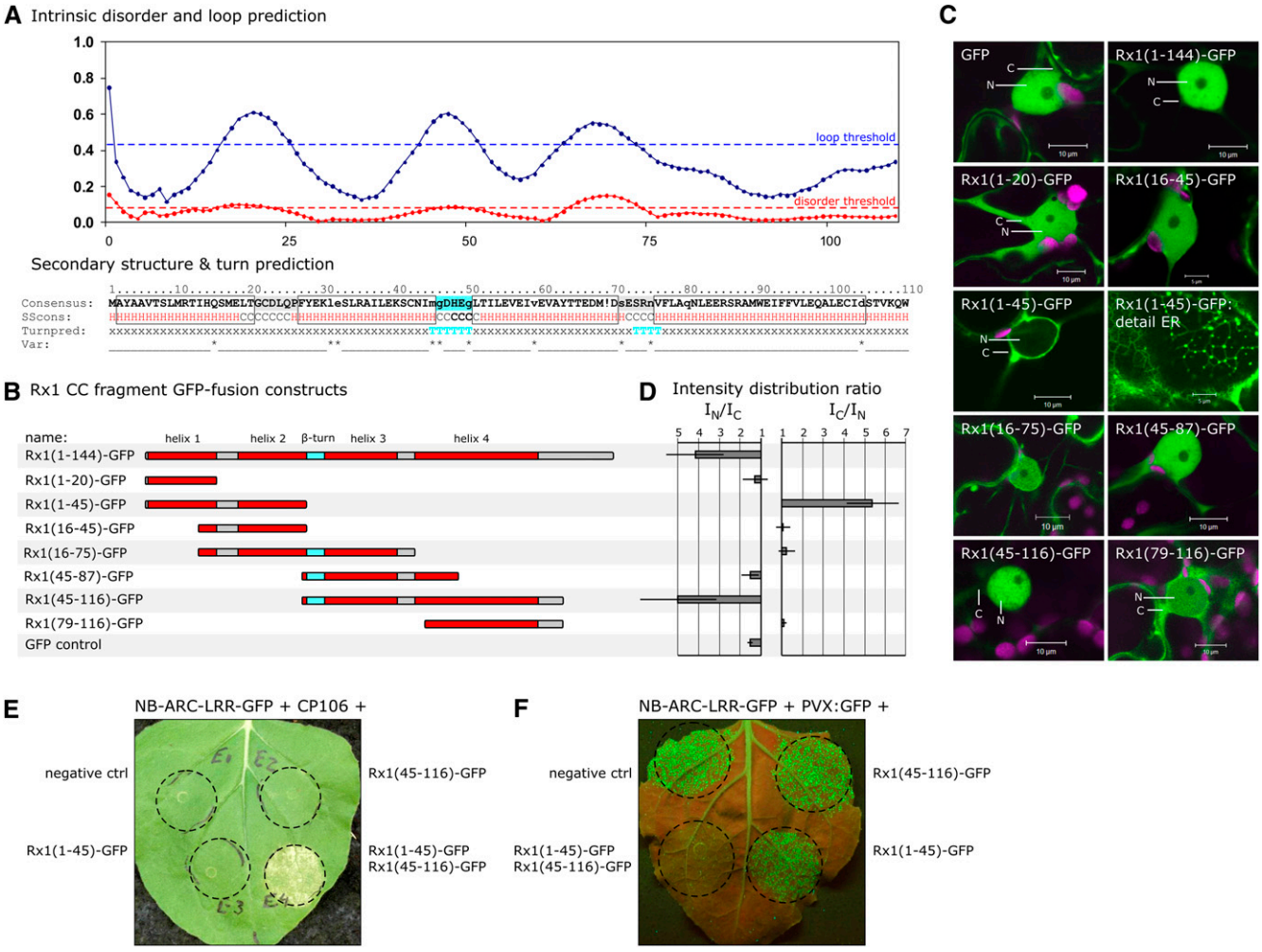

Figure 6. Subcellular Localization of Fluorescent Fusion Proteins of Secondary Structure–Based CC Domain Fragments of Rx1.

(A) Consensus secondary structure propensity of the CC domain suggests the presence of four α-helices (H, shown in red) joined by three stretches that show a high intrinsic disorder propensity defined both by the inability to form secondary structure (coils, in blue) and high B-factors (hot-loops, in red). In addition, the CC sequence shows a high propensity for a β-turn structure especially between helices 2 and 3 (T, shown in blue).

(B) Schematic representation of the constructed Rx1 CC fragments, which were all fused to GFP at the C terminus. The predicted secondary structure is indicated in color: α-helices in red and the central β-turn in blue. The amino acid positions corresponding with the fragments sequence in the full CC domain are noted in the fragment names.

(C) Confocal images showing the subcellular localization patterns for each CC fragment. For fragment Rx1(45-116)-GFP, a similar nuclear localization was observed like shown for the full CC domain [Rx1(1-144)-GFP]. For Rx1(1-45)-GFP, fluorescence was exclusively located in the cytoplasm associated with endoplasmic reticulum and Golgi-like structures (a detail of this cytoplasmic localization pattern is shown). The other fragments were shown to be located in both the nucleus (N) and the cytoplasm (C) comparable to free GFP.

(D) Fluorescence intensity distribution ratio showing the nuclear (I_N/I_C) or cytoplasmic (I_C/I_N) localization of each CC fragment. Average intensities were determined in confocal images using the image analysis application ImageJ. Ratios shown are the averages (±SD) for 8 to 10 cells.

(E) In trans complementation HR assay. If the CC fragments Rx1(1-45)-GFP and Rx1(45-116)-GFP are coexpressed with the NB-ARC-LRR-GFP construct (amino acids 144 to 937), a functional Rx1 is reconstituted that initiates a cell death response in the presence of the PVX CP.

(F) Transient PVX resistance assay. Combinations of the NB-ARC-LRR-GFP construct and the CC fragments Rx1(1-45)-GFP and Rx1(45-116)-GFP were coexpressed with PVX:GFP. PVX accumulation was visualized by the GFP expression at 5 d after infiltration.

nucleus (Thompson et al., 2002; Houtsmuller, 2005). As expected, we observed the highest diffusion coefficients for the free GFP (Figure 7D). For the full CC domain, a significantly smaller diffusion coefficient was measured (Figure 7D). Rx1(45-116)-GFP had an effective diffusion coefficient ~3 to 4 times lower than free GFP and, thus, even lower than the diffusion coefficient derived for the full CC domain. Rx1(45-87)-GFP and Rx1(79-116)-GFP, which encompass sequences corresponding to parts of the Rx1(45-116)-GFP construct, gave diffusion coefficients intermediate to the values for GFP and the CC-GFP but still

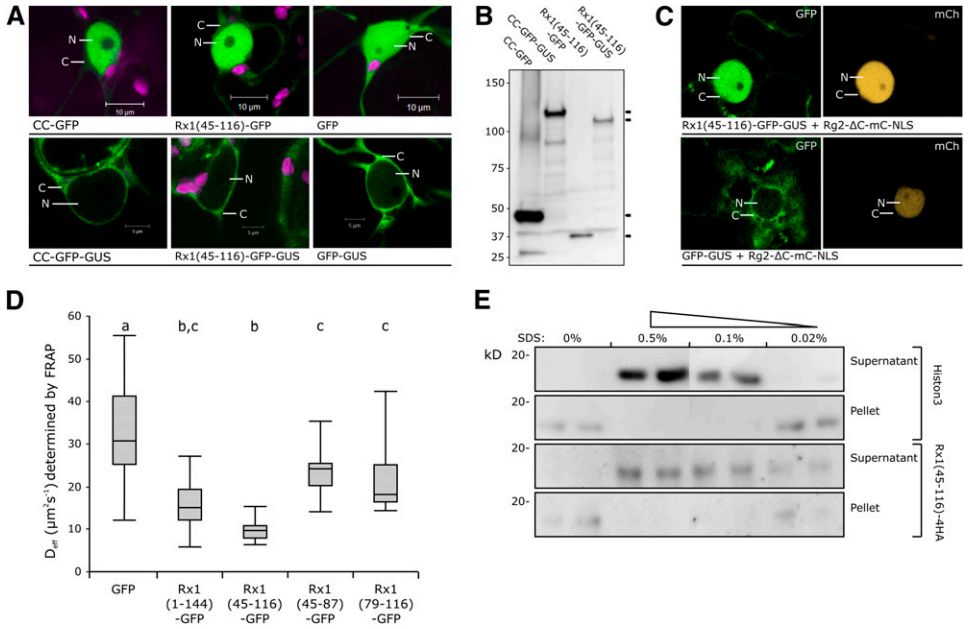

Figure 7. Diffusional Behavior of Rx1 CC Fragments in the Nucleus.

(A) Confocal images of the subcellular localization of single GFP fusion constructs of the CC (top panels) and the equivalent GFP-GUS fusion constructs (bottom panels). Nucleus (N) and cytoplasm (C) are indicated.

(B) Anti-GFP immunoblot of the GFP-GUS fusion constructs to show the integrity of the constructs. The constructs were transiently expressed in *N. benthamiana* leaves.

(C) Rx1(45-116)-GFP-GUS and GFP-GUS coexpressed with a nuclear targeted version of the RanGAP2 N-terminal WPP domain (WPP-mCh-NLS). GFP fluorescence is displayed in green (left panels) and mCherry fluorescence in orange (right panels).

(D) Effective diffusion coefficients (Deff) of GFP, Rx1(1-144)-GFP (CC-GFP), Rx1(45-116)-GFP, Rx1(45-87)-GFP, and Rx1(79-116)-GFP as derived from FRAP measurements in the nucleus of *N. benthamiana* cells ($n = 20$, except for GFP, $n = 35$), 2 d after agroinfiltration. For the fragment Rx1(45-116)-GFP and the full CC domain (Rx1-1-144)-GFP), a significant slower diffusion was observed compared with the other tested fragments and free GFP. The distribution of data points is depicted in a box plot. The means were statistically analyzed with the Tukey test and grouped (a, b, and c) according to significant differences at α 0.01.

(E) Rx1(45-116)-4HA extracted from purified nuclei by sonication in buffers with increasing SDS concentrations (0, 0.02, 0.1, and 0.5%). After sonication, both the soluble fraction and an insoluble pellet were boiled in loading buffer and separated by SDS-PAGE. The sonication disrupts the nuclei (checked by microscopy) but does not release the Rx1 CC fragment (or the DNA bound Histone 3) in the soluble fraction. The addition of increasing levels of SDS in the sonication buffer results in an increasing amount of Rx1(45-116)-4HA in the soluble fraction. Every treatment was tested in duplo.

diffused significantly faster than fragment Rx1(45-116)-GFP. Thus, the strong nuclear localization of CC-GFP and Rx1(45-116)-GFP coincided with a significantly slower diffusion in the nucleus.

Another indication for such nuclear interaction of the CC or the CC fragment Rx1(45-116)-GFP are the conditions under which these proteins can be released from purified nuclei. Purified nuclei were sonicated in the absence or presence of increasing concentrations of the anionic detergent SDS. Even sonication in a buffer without SDS disrupted the nuclei, which was confirmed by microscopy. However, only in the presence of 0.1 or 0.5% SDS was Rx1(45-116)-4HA released into the solution (Figure 7E). Histone 3, which was detected with specific antibodies as an example of a DNA bound protein, was released under similar conditions (Figure 7E).

These results suggest that the nuclear accumulation of the CC protein and Rx1(45-116)-GFP can be explained by transient binding with relatively immobile nuclear structures.

DISCUSSION

In this study, we have shown that the CC-NB-ARC-LRR R protein Rx1 has a nucleocytoplasmic distribution in the cell and that both the nuclear and cytoplasmic pools of Rx1 are required for full functionality. A remarkable qualitative difference was observed between the subcellular Rx1 pools; retargeting Rx1 toward the nucleus impacts virus resistance more than shifting the Rx1 localization to the cytoplasm. The strongest decrease in Rx1 functioning was seen when the elicitor of Rx1, PVX CP, was forced to accumulate exclusively in the nucleus. We conclude from the ensuing loss of Rx1 activation that elicitor recognition has to take place in the cytoplasm. Interestingly, the domain deletion constructs and the P-loop mutant of Rx1 demonstrated that the LRR domain, which has a role in elicitor recognition, is also associated with a cytoplasmic localization. The CC domain, on the other hand, is needed, either directly or indirectly, for the nuclear localization of the Rx1 protein, although it lacks

discernable transferable NLS sequences. Constructs based on the predicted secondary structure revealed a minimal functional CC domain fragment that shared the nuclear accumulation with the full-length CC. Both this CC fragment (amino acids 45 to 116) and the full-length CC were shown to have a lower diffusion coefficient in the nucleus than would be expected from their size. The most likely explanation for this behavior is the occurrence of transient interactions with yet unknown relatively immobile nuclear components.

Rx1 Is Activated in the Cytoplasmic Compartment

In the past few years, the subcellular localization of several R proteins has been determined by imaging their GFP fusion products or by cell fractionation studies. NB-LRR R proteins, originally thought to be cytoplasmic, exhibit an unexpected variety in subcellular localization from association to the plasma membrane (Boyes et al., 1998) and to the endoplasmic reticulum (Weaver et al., 2006; Wang et al., 2007) to a nucleocytoplasmic distribution (Shen and Schulze-Lefert, 2007). Barley MLA, tobacco N, and *Arabidopsis* RPS4 all showed a clear loss of function when their nuclear localization was prevented either by the addition of exogenous NESs (Burch-Smith et al., 2007; Shen et al., 2007) or by mutations of an endogenous NLS (Wirthmueller et al., 2007). Judged by the resistance phenotypes of Rx1 targeted to the cytoplasm or the nucleus, Rx1 needs to be distributed among both compartments for full functionality. It is interesting to note that RanGAP2, which interacts with the CC domain of Rx1, has an almost exclusive cytoplasmic localization (Rose and Meier, 2001; Pay et al., 2002; Jeong et al., 2005; Sacco et al., 2007; Tameling and Baulcombe, 2007). Although silencing *RanGAP2* in *N. benthamiana* compromised Rx1-mediated resistance (Tameling and Baulcombe, 2007) and overexpression of RanGAP2 caused the elicitor-independent activation of Rx1 CC-NB fragments (Sacco et al., 2007), the precise function of the RanGAP2 interaction with Rx1 is still unknown. RanGAP2 also interacts with the CC domain of Gpa2, a close homolog of Rx1, which can be activated by certain RanBPM-like proteins (RBPs) secreted by the nematode *Globodera pallida*. The finding that Gpa2 activation is stimulated by the stabilization of an interaction between the nematode RBPs and RanGAP2 indicates that the latter could have a role as a guarded host protein facilitating Gpa2-mediated recognition of the RBPs (Collier and Moffett, 2009; Sacco et al., 2009). If this is true, and a similar indirect RanGAP2-mediated recognition underlies PVX CP recognition, then this would explain why the nuclear-targeted PVX CP no longer activates Rx1. However, a study by Tameling et al. (2010) determining the link between RanGAP2 localization and Rx1 functioning demonstrated that when the RanGAP2 WPP domain itself is targeted to the nucleus by an NLS fusion, thereby pulling Rx1 into the nucleus as well, it still does not allow Rx1 activation in the nuclear compartment. However, it might be the full-length RanGAP2 that is required for elicitor recognition.

If R proteins recognize pathogen-derived elicitors directly or indirectly via guarded host proteins, then the proximity in the same compartment of all components involved in the recognition is a prerequisite (Martin et al., 2003). The small size of PVX CP allows it to move freely between the nuclear and cytoplasmic compartment (Figure 3A). Thus, the CP localization by itself does not exclude the nucleus as the compartment where recognition could take place. It is tempting to speculate that the roles the CP fulfills in PVX replication and cell–cell movement of viral RNA (Oparka et al., 1996; Fedorkin et al., 2001; Karpova et al., 2006; Bamunusinghe et al., 2009), which have been associated with the endomembrane system and plasmodesmata, form the ground for its recognition in the cytoplasm.

Several recent examples demonstrate how closely subcellular localization and R protein–mediated recognition mechanisms can be linked. The *Tobacco mosaic virus* helicase p50 effects a change in the localization of the host protein NRIP1, as it releases it from the chloroplast stromules to the cytoplasm and nucleus. Only then can the tobacco R protein N interact with NRIP1 via its TIR domain (Caplan et al., 2008b). The effector PopP2 is secreted by *R. solanacearum* into the host cells, where it is transported into the nucleus via its NLS. A host protein, the Cys protease RD19, directly interacts with PopP2. In the presence of PopP2, the RD19 protein changes its localization from the putative prevacuolar vesicles to the nucleus (Bernoux et al., 2008). A GFP-fused version of the *Arabidopsis* resistance protein RRS1-R could not be detected in the absence of PopP2 (its cognate elicitor), but when RRS1-R was coexpressed with PopP2, both colocalized in the nucleus (Deslandes et al., 2003).

Recently, the *Arabidopsis* immune regulator protein EDS1 was shown to be balanced between the nucleus and the cytoplasm (García et al., 2010). EDS1 plays an important role in signaling of basal defense and TIR-NB-LRR R protein-induced defense (Aarts et al., 1998). It forms complexes with the defense signaling proteins PAD4 and SAG101 in the cytoplasm and nucleus (Feys et al., 2001, 2005). The nuclear pool of EDS1 increases during the RPS4-triggered immune response and is associated with transcriptional reprogramming (García et al., 2010). However, even during defense a cytoplasmic pool is retained. Redirecting EDS1 to a more cytoplasmic localization via an NES reduced RPS4 triggered resistance and basal defense responses. It was concluded that both the cytoplasmic and nuclear pools of EDS1 have specific functions in the immune response.

The CC and LRR Domains Play Distinct Roles in the Nucleocytoplasmic Distribution of Rx1

If the presence of Rx1 in both compartments is needed for full resistance, then the mechanisms determining this distribution are of interest. We demonstrated that preventing nucleotide binding to the NB-ARC by mutating the conserved Lys (K176R) in the P-loop abolishes the nuclear localization of full-length Rx1. The bound nucleotide (ADP or ATP) determines the overall structure of an NB-LRR R protein by interacting with motifs in the NB, ARC1, and ARC2 domains (Takken et al., 2006). It was shown earlier that this P-loop mutation disrupts the intramolecular interaction between the CC and the NB-ARC-LRR of Rx1 but not the interaction between the LRR and the CC-NB-ARC (Moffett et al., 2002; Leister et al., 2005). The effects of the CC deletion, the P-loop mutation, and the effect of silencing of *SGT1* on the localization of Rx1 indicate that the structure and conformation of the various Rx1 domains play a role in balancing Rx1 between the nuclear and cytoplasmic protein pools. As an

additional control, GFP-Rx1 was coexpressed with an NLS-tagged version of the interacting RanGAP2 WPP domain in *SGT1*-silenced plants (see Supplemental Figure 4 online). The induced relocation of Rx1 to the nucleus indicates that in *SGT1*-silenced plants, Rx1 is still able to take part in the RanGAP2 interaction and can enter the nucleus if directed there via the nuclear import system.

SGT1 forms a chaperone complex with RAR1 and HSP90, which is essential for NB-LRR protein folding and stability (Takahashi et al., 2003; Holt et al., 2005; Botër et al., 2007; Shirasu, 2009). The chaperone function of SGT1 and RAR1 for NB-LRR proteins has earlier been associated with the LRR domain; for example, the RAR1 dependence of barley MLA variants is determined by their LRR (Bieri et al., 2004). SGT1 has been shown to localize in both the cytoplasm and the nucleus (Noël et al., 2007). For the nuclear localization, it requires a complete SGS domain, which functions as interaction domain for HSC70. The chaperone HSC70 can actively be transported to the nucleus via an NLS and has been shown to play a role in nucleocytoplasmic shuttling in several eukaryotic systems (Kose et al., 2005; Cazalé et al., 2009). Similarly, HSP90 plays a role in nucleocytoplasmic shuttling of, among others, metazoan nuclear receptors like the glucocorticoid receptor (Kang et al., 1994; Tago et al., 2004; Echeverría et al., 2009). Further experiments are needed to elucidate the role that the SGT1-RAR1-HSP90 chaperone complex plays in Rx1 nucleocytoplasmic balancing.

RanGAPs, like the Rx1 interactor RanGAP2, have a well-described role in the main nucleocytoplasmic shuttling machinery (Merkle, 2003; Stewart, 2006; Cook et al., 2007). The GTPase Ran travels to the nucleus in its GDP-bound form and from the nucleus to the cytoplasm in its GTP-bound form (Görlich et al., 1996). The interaction of RanGTPase with RanGAP in the cytoplasm strongly stimulates its GTPase activity, which helps it to return to the GDP-bound state. However, no evidence exists that RanGAPs themselves can shuttle proteins from the cytoplasm to the nucleus; therefore, it is not likely that RanGAP2 has a direct role in the transport of Rx1 to the nucleus. On the other hand, a detailed study on the effect RanGAP2 has on the subcellular localization and activation of Rx1 (Tameling et al., 2010) showed that RanGAP2 affects the nucleocytoplasmic partitioning of Rx1 but does not require GAP (GTPase activating protein) activity to produce this effect.

Still, Rx1 has a mass well above the passive nuclear import threshold (~110 kD without and ~140 kD with GFP fusion). Proteins with a molecular mass higher than 40 kD (or a Stokes radius over 2.7 nm, as dimensions are more important than molecular mass) are limited in their passive passage through the nuclear pore complex (Paine et al., 1975; Merkle, 2003; Mohr et al., 2009). Therefore, it is likely that the transport of NB-LRR resistance proteins in and out of the nucleus needs to be actively facilitated. A number of NB-LRR proteins do indeed contain classical NLS sequences, as was noticed in the analysis of the R proteins encoded in the poplar genome (Tuskan et al., 2006; Kohler et al., 2008). A large fraction of the CC-NB-LRR and TIR-NB-LRR proteins encoded in the *Arabidopsis* genome contain predicted mono- and bipartite NLS sequences (Shen and Schulze-Lefert, 2007). The requirement of a bipartite NLS for nuclear targeting and resistance signaling has been demonstrated for *Arabidopsis* TIR-NB-LRR RPS4 and SNC1 (Wirthmueller et al., 2007; Cheng et al., 2009). The RPS4 NLS does not direct the complete pool of RPS4 to the nucleus; a substantial cytoplasmic subpool (90%) is still present in association with the endomembrane system. The localization of the autoactive TIR-NB-LRR mutant snc1 was shown to shift to the cytoplasm in *Arabidopsis* carrying a mutation in Nucleoporin88, which was associated with a reduced snc1 activity (Cheng et al., 2009).

Most classical NLSs are linear Arg- and Lys-rich sequence motifs, mediating the interaction with variants of the nuclear transport receptor importin-α. NLSs can also be formed by a combination of residues that lie further apart in the primary sequence but are brought close to each other in the three-dimensional structure. Even signals based on residues from two separate, interacting, polypeptides have been reported, like in the STAT1 dimer (Fagerlund et al., 2002). Such a complex NLS based on a discontinuous stretch of residues cannot easily be detected without detailed information on the three-dimensional structure of the protein and an extensive screen for interactions with the various importins.

Like Rx1, tobacco N and barley MLA are present in the nucleus but do not contain recognizable classical NLSs (Burch-Smith et al., 2007; Shen et al., 2007). We found that although the CC domain is required for the nuclear localization of Rx1, it does not contain an autonomous import signal that can actively transport a GFP-GUS fusion product into the nucleus (Figure 7A). It should be noted that in yeast, only 57% of the nuclear proteins contains a classical NLS (Lange et al., 2007). The remaining 43% of nuclear proteins is thought to pass the nuclear pore complex via alternative mechanisms, like direct interactions with importin β or nucleoporins, nonclassical nuclear targeting signals, or cotransport via interactions with proteins that do contain NLSs, the so-called piggyback mechanism (Ursula Stochaj, 1999; Christophe et al., 2000; Dostie et al., 2000; Cingolani et al., 2002; Xu and Massagué, 2004; Lee et al., 2006; Chuderland et al., 2008; Lange et al., 2008).

Nuclear Accumulation of the CC Can Be Attributed to a Small Functional and Structural Subdomain

To study the role of the CC in the nuclear accumulation of Rx1, a structural analysis was conducted. Surprisingly little has been reported on the structure of the R protein CC domain (or non-TIR domain). In the CC domain of proteins encoded by some of the first R genes to be cloned, an amphipathic heptad repeat was recognized (Bent et al., 1994; Grant et al., 1995; Bendahmane et al., 1999). Such heptad repeats consist of regularly spaced hydrophobic residues that, if present in an α-helix, will form a hydrophobic surface along one side of the structure. In combination with bordering polar/hydrophilic residues, these hydrophobic areas form the interaction surface between helices in a CC structure (Cohen and Parry, 1986; Lupas, 1997). Computational analysis of the primary amino acid sequence shows that the Rx1 CC domain indeed mainly consists of α-helices interspersed by loop regions and likely a β-turn around amino acid 45. The in trans functionality of the CC fragments split at this predicted β-turn indicates that both CC fragments reconstitute a functional CC and thus likely interact. A similar in trans

functionality has been shown before for Rx1 split between the CC and NB and between the ARC2 and LRR region and corresponded with an interaction in these cases (Moffett et al., 2002). Further experiments will be needed to determine if this is a direct interaction and to determine the role of the amphipathic heptad repeat in this interaction. The CC domain of Rx1 is involved in at least two known interactions: an intramolecular interaction with the NB-ARC-LRR domains (Moffett et al., 2002; Rairdan et al., 2008) and an intermolecular interaction with the N-terminal WPP domain of RanGAP2 (Sacco et al., 2007; Tameling and Baulcombe, 2007). By mutagenesis, it was shown that the interaction with the NB-ARC-LRR was mainly determined by the conserved EDMVD motif and the interaction with the RanGAP2 by the region surrounding this motif (Rairdan et al., 2008). In our secondary structure model, the EDMVD motif falls within the 3rd α-helix, and it is interesting to note that the regions essential for the NB-ARC-LRR and RanGAP2 interactions are both situated within the minimal CC fragment that displays the strong nuclear accumulation and slow nuclear diffusion phenotype.

FRAP has been applied extensively in the study of nuclear protein dynamics (Carrero et al., 2003; Houtsmuller, 2005; McNally and Kevin, 2008). The recovery kinetics reflect the mobility of the fluorescent protein, which itself is influenced by several factors like the dimensions of the protein, the viscosity of the solution, and the interaction kinetics of the protein. The difference in the effective diffusion coefficient observed for the CC-GFP and Rx1(45-116)-GFP products in comparison with free GFP cannot be explained only by the difference in their molecular mass. Molecules of up to 500 kD are not hindered by nuclear structures and have been shown to diffuse unrestrictedly in the nucleus (Seksek et al., 1997; Görisch et al., 2005). Furthermore, the size dependency of the diffusion coefficient is small; for globular proteins, the diffusion coefficient is proportional to the inverse of the cube root of the molecular mass ($D \sim M^{-1/3}$) (Reits and Neefjes, 2001; Mueller et al., 2010). This implies that to be able to explain the difference in the observed diffusion coefficient between free GFP (32.7 $\pm$ 10.3 $\mu m^2\ s^{-1}$, 27 kD) and Rx1 (45-116)-GFP (10.0 $\pm$ 2.7 $\mu m^2\ s^{-1}$, 34 kD) (Figure 7D), the latter should have a mass of $\sim$30 times higher than free GFP.

The most plausible explanation for the diffusional behavior of the CC-GFP and Rx1(45-116)-GFP constructs appears to be transient binding to a less mobile component in the nucleus. Similar diffusional behavior has been found for many chromatin-associated proteins, which led to the idea that most proteins recruited to the chromatin are only binding transiently and show rapid turnover kinetics (Phair et al., 2004; Gorski et al., 2006; Launholt et al., 2006; Hager et al., 2009). A more extensive FRAP analysis than performed here could even provide information about binding kinetics, like the "on" and "off" rates and the relative number of binding sites (Sprague et al., 2004; Sprague and McNally, 2005; Beaudouin et al., 2006). The fact that, like the histone 3 control, the CC fragment Rx1(45-116)-4HA is only released from purified nuclei after sonication in a buffer containing SDS supports the hypothesis that it takes part in an interaction in the nucleus. To what protein or structure the Rx1 CC binds, assuming that the nuclear full-length Rx1 takes part in the same interaction, and what the role of this in Rx1 mediated signaling is will be the focus of further studies.

A relatively small, but consistent, suppressive effect on the functioning of Rx1 was observed after artificially shifting Rx1 out of the nucleus through fusion to an NES. Therefore, we can assume that some part of Rx1 signaling does take place in the nucleus, and it is tempting to speculate that this might be linked to the CC domain. The discovery of the R protein RRS1-R suggested that R proteins could be directly involved in transcriptional regulation via transcription factors (Lahaye, 2002). It consists of TIR, NB-ARC, and LRR domains with a C-terminal fusion to a WRKY domain, characteristic of the WRKY class of transcription factors (Deslandes et al., 2002). The *Arabidopsis* R protein RPS4 has recently been shown to operate only in combination with RRS1-R. The RPS4/RRS1-R pair confers resistance against strains of *Pseudomonas syringae*, *R. solanacearum*, and the fungus *Colletotrichum higginsianum* (Narusaka et al., 2009). Maybe RPS4 indirectly uses the WRKY domain of RRS1-R for its functioning. In addition, the CC domain of MLA has been shown to interact with a WRKY transcription factor in a yeast two-hybrid screen. The interaction between full-length MLA and this WRKY protein was enhanced in the presence of a *Blumeria*-derived elicitor (Shen et al., 2007). The WRKY factor interacting with MLA functions as a suppressor of basal resistance. It was hypothesized that the interaction with MLA leads to derepression of basal resistance signaling. Finally, even N-terminal domains of the plasma membrane–associated CC-NB-LRR protein RPM1 were shown to interact with TIP49a, a nuclear factor involved in the transcriptional machinery and chromatin remodeling (Holt et al., 2002; Gallant, 2007). Hence, it is tempting to infer from these examples that the nuclear localization of Rx1 might be similarly linked to transcriptional regulation of downstream signaling pathways, of which the mechanism has not been elucidated yet.

METHODS

Sequence and Secondary Structure Characterization

Similarity searches were performed with BLAST using Blosum62. Patterns, profiles, and domain recognition were scanned with InterPro (Quevillon et al., 2005) and CDART (Geer et al., 2002), which integrates Pfam, Prints, Prodom, SMART, TIGR, and Prosite databases. Secondary structure predictions were performed with methods best ranked in CASP4:SOPMA (Geourjon and Déleage, 1995), GOR IV (Garnier et al., 1996), PsiPred (Jones, 1999), Jpred (Cole et al., 2008), HNN (Guermeur, 1997), and PROF (Ouali and King, 2000). Specialized β-turn prediction was performed with BETATURNS (Chou, 2000). Domain linker prediction was performed using the Domain Linker Predictor (Miyazaki et al., 2002). Intrinsic disorder prediction was performed with DisEMBL (Linding et al., 2003).

Expression Cassette Construction

The sequences of all applied oligonucleotides are listed in Supplemental Table 1 online.

35S Promoter Constructs

The Rx1 encoding sequences, including introns, were inserted in the plant expression vector pRAP (Schouten et al., 1997). Rx1 was amplified using the primers 5GpRxbn and Rxrev and transferred to *Nco*I-*Sal*I–digested

pRAP, resulting in pRAP:Rx1. To create the leaky scan (35SLS) Rx1 construct, the Rx1 sequence was amplified using the RxLSFor and Rxrev and cloned to pRAP via *Nco*I and *Sal*I.

Endogenous Promoter Constructs

Comparison of the genomic sequence of Rx1 (GenBank AJ011801) and the homologous Gpa2 (GenBank AF195939) showed extensive similarity in the promoter and transcription terminator regions. These regions of similarity were taken as the basis for creation of vectors carrying endogenous transcription cassettes in a pUC19 background. The Rx1 3′-untranslated region (UTR) (transcription termination) region (274 bp) was amplified from pBIN:BAC-Rx1 (pBIN+:RGC4; van der Vossen et al., 2000) template using the primers 5UTRkp and 3UTRrev and cloned as a *Kpn*I-*Pac*I fragment into pRAP:YFP, replacing the Tnos. The Rx1 promoter region (2804 bp between *Xba*I and ATG start codon) was constructed in two steps. First, the region between the *Dra*III site (nucleotide 1429) and the start codon was amplified from pBIN:BAC-Rx1 (pBIN+:RGC4) using the primers bRxAdeIf and RxbnREV. This 1396-bp *Dra*III-*Nco*I fragment was cloned alongside the 1431-bp *Asc*I-*Dra*III fragment of pBIN:BAC-Rx1 into pRAP:YFP with Rx1 3′-UTR, from which the 35S region was removed by *Asc*I-*Nco*I digestion. The resulting vector pRXI:YFP drives expression of a reporter gene. *R* gene constructs were exchanged between pRAP and pRXI using the unique *Nco*I and *Pst*I sites.

Cloning R *Gene Fusion Partners*

The YFP (enhanced YFP; Clontech), CFP (enhanced CFP; Clontech), and GFP (enhanced GFP; Clontech) (Yang et al., 1996) reporter genes were amplified by PCR using the primers 5CFPsbn and 3CFPsrk. PCR products were cloned as a *Nco*I-*Kpn*I fragment in the vector pRAP between the 35S promoter and Tnos termination regions.

C-Terminal Fusions

In the plant expression vector pRAP:cbp (cbp is a stuffer fragment), the *Sph*I-*Pac*I segment is replaced by the annealed oligos CBPY1+2 with *Sph*I-*Nco*I overhang and the YFP-Tnos *Nco*I-*Pac*I fragment. In the resulting pRAP:cbp-YFP, the fluorescent protein is preceded by *Not*I and *Sal*I. The *Sal*I-*Sst*I GFP fragment, derived from pCR2.1:GFP, is cloned into pRAP:cbp-YFP. In the resulting vector, an extra *Bam*HI site is available for fusions. To create the GFP-GUS constructs, GUS was isolated from pGEM-T:GUS via *Nco*I-*Spe*I and ligated to pRAP:GFP, pRAP:CC-GFP, and pRAP:Rx1(45-116)-GFP via *Bsp*HI-*Xba*I.

Targeting Signals

The SV40 NLS (Lanford and Butel, 1984; Haasen et al., 1999) was generated as an annealed oligo (SV1 + SV2) with *Nco*I-*Nhe*I overhang. It was cloned into pRAP:YFP-HA8 (*Nco*I-*Nhe*I), resulting in pRAP:NLS-HA8. In the mutated control version pRAP:nls*-HA8, the oligo pair SVmut1 and SVmut2 was used. The vectors pRAP:GFP-NLS-HA8 and pRAP:GFP-nls*-HA8 were created by introduction into pRAP:NLS-HA8 and pRAP:nls*-HA8 (*Asc*I-*Nco*I) of the 35S:GFP (*Asc*I-*Bsp*HI fragment). As an NES, the sequence from PKI (Wen et al., 1995) was used. The annealed oligo pair PK1 + PK2 with *Sst*I-*Nhe*I overhang was cloned in between the same sites in pRAP:GFP-HA8. The mutated version was inserted in a similar way. The resulting plasmids are pRAP:GFP-NES-HA8 and pRAP:GFP-nes*-HA8.

R *Gene–Derived Segments*

In pRAP:Rx1, digested with *Asc*I-*Nco*I, the 35S:YFP (*Asc*I-*Sst*I) fragment is ligated alongside the annealed oligo linker12 (linker 12for +, linker12rev) (amino acid sequence 5′-GGGSGGGSGGGS-3′). From the resulting pRAP:YFP-Rx1, an N-terminal GFP version is prepared by exchange of YFP for GFP via *Nco*I-*Sst*I. Via *Nco*I-*Pst*I, pRXI:GFP-Rx1 was prepared. To allow C-terminal fusions, Rx1 cDNA was prepared. The primer combination 5RxexFor and 3Rxnot amplified the Rx1 C-terminal end, which was then cloned into pCR2.1Topo and recloned as *Bsp*EI-*Kpn*I fragment in pRAP *Nco*I-*Kpn*I and the Rx1 *Nco*I-*Bsp*EI fragment. Finally, in the cDNA version of pRAP:Rx1, digested with *Not*I-*Pac*I, the GFP-Tnos from pRAP:cbp-GFP was inserted, leading to pRAP:Rx1-GFP. $35S_{LS}$:Rx1-GFP was created following the same strategy. To create the GFP-NLS/nls*-Rx1 constructs, pRAP:GFP-Rx1 was opened with *Nco*I-*Bam*HI, and the GFP-NLS or GFP-nls* segment from pRAP:GFP-NLS or -nls* (*Nco*I-*Bam*HI) was ligated. For introduction of the NES, the *Asc*I-*Bam*HI fragment from pRAP:GFP-NES or -nes* was introduced in *Asc*I-*Bam*HI–digested pRAP:GFP-Rx1. The GFP-NLS/nls*-Rx1 insert from the pRAP versions was introduced into pRXI using *Nco*I-*Pst*I. For the GFP-NES/nes*-Rx1 in pRXI:GFP-Rx1, the *Sst*I-*Cla*I fragment was exchanged for the *Sst*I-*Cla*I fragments from pRAP:GFP-NES-Rx1 and GFP-nes*-Rx1. The $35S_{LS}$:Rx1-GFP-NES/nes*-8HA and $35S_{LS}$:Rx1-GFP-NLS/nls*-8HA constructs were created by exchanging the GFP in 35SLS:Rx1-GFP via SstI-PacI for the GFP-NES/nes*/NLS/nls*-8HA fragments from the pRAP:GFP-NES/nes*/NLS/nls*-8HA constructs. The P-loop mutant Rx1 K176R was generated by splicing by overlap extension of CC-NB-ARC fragments amplified with the primer combinations 5GpRxbn + 3LysRrev and 5LysRfor and 3NBSeRev on Rx1 template. This CC-NB-ARC K176R segment was introduced into full-length Rx1 constructs.

LRR Constructs

The sequence encoding the Rx1 LRR domain from amino acid 473 was amplified from cDNA using the primers For-LRRrx-1 and Rev-LRRrx-1 and then cloned into pBAD-topo (Invitrogen). In this vector, the LRR is preceded by the extra amino acids MGSGSGDDDDKLAL. Full-size pBAD:Rx1 was obtained by insertion of the *Nco*I-*Cla*I fragment from pRAP:Rx1. From pBAD:LRR, the *Nco*I-*Cla*I fragment was cloned into pRAP:Rx1 (*Nco*I-*Cla*I), resulting in pRAP:LRR. In this vector, the GFP sequence was introduced as a *Nco*I-*Bam*HI fragment taken from pRAP:GFP-Rx1. GFP and the LRR are connected by the linker GGGSGGGSGDDDDKLAL.

CC-NB-ARC Constructs

The Rx1 CC-NB-ARC (amino acids 1 to 474) encoding sequence was amplified from Rx1 template using the primer set 5GpRxbn and NBSerev and then cloned into pRAP via *Nco*I-*Kpn*I restriction sites. A C-terminal fusion of YFP was accomplished by inserting into the *Asc*I-*Nco*I cut pRAP:YFP the *Asc*I-*Eco*RI fragment of pRAP:CC-NB-ARC and a linker peptide encoding *Eco*RI-*Nco*I fragment annealed from Ctyfp1 and Ctyfp2. In the resulting plasmid, pRAP:CC-NB-ARC-YFP, the linker SGGSGGGGSGGGGS connects CC-NB-ARC and YFP. pRAP:CC-NB-ARC-GFP was created by exchanging YFP for GFP from pRAP:NB-ARC-GFP via *Apa*LI-*Pac*I. The vector pRAP:YFP-CC-NB-ARC is created by introducing the *Stu*I-*Pac*I fragment from pRAP:CC-NB-ARC into pRAP:YFP-Rx1. The GFP-CC-NB-ARC K176R *Asc*I-*Apa*LI fragment and the *Apa*LI-*Pac*I fragment from pRAP:NB-ARC-GFP were inserted into *Asc*I-*Pac*I–digested pRAP, resulting in pRAP:GFP-CC-NB-ARC-GFP K176R. Then, the *Asc*I-*Hpa*I fragment was replaced by *Asc*I-*Hpa*I from pRAP:Rx1, leading to pRAP:CC-NB-ARC-GFP K176R. To amplify the NB-ARC region of Rx1, the primer pair 5NBSf and ApaLRev was used. The amplified product was cloned as a *Nco*I-*Kpn*I fragment into pRAP. To enable C-terminal fusions, the annealed oligo AN1 +AN2 was introduced via *Apa*LI-*Kpn*I. The resulting pRAP:NB-ARC-an carries a *Not*I site and allowed cloning of the GFP-Tnos *Not*I-*Pac*I fragment to yield pRAP:

NB-ARC-GFP. In this construct, the Rx1 segment extends from amino acid 142 to 489.

CC Deletion Construct

To create the CC deletion of Rx1-GFP, the *Asc*I-*Apa*LI fragment from pRAP:NB-ARC-an was joined alongside the *Apa*LI-*Pac*I fragment from pRAP:Rx1 in *Asc*I-*Pac*I–digested pRAP, resulting in pRAP:NB-ARC-LRR-GFP.

CC-GFP and CC Fragments

The CC domain of Rx1 was amplified from Rx1 template using the primer combination 5GpRxsbn and 3CCnot. The fragment was cloned via *Nco*I-*Kpn*I and into pRAP. Then, after *Not*I-*Pac*I digestion, the GFP-Tnos fragment from pRAP:cbp-GFP was introduced, leading to pRAP:CC-GFP. To create pRAP:CC-3GFP, the *Asc*I-*Bsp*HI CC-GFP fragment was fused to the *Nco*I-*Pac*I GFP2-Tnos segment from pRAP:cbp-GFP2 in the vector pRAP (*Asc*I-*Pac*I). CC fragment constructs were prepared by amplification of Rx1 template with the following primer combinations: Rx1 (1-45), 5GpRxsbn and Rev-BamHI-AC; Rx1(1-20), 5GpRxsbn and Rev-BamHI-B; Rx1(16-45), For-nco-CD and Rev-BamHI-AC; Rx1(45-89), For-nco-EG and Rev-BamHI-ED1; Rx1(79-116), For-nco-F and Rev-BamHI-GF; Rx1(45-116), For-nco-EG and Rev-BamHI-GF. All these PCR fragments were ligated as a *Nco*I-*Bam*HI fragment with the pRAP *Asc*I-*Nco*I fragment into the *Asc*I-*Bam*HI–digested pRAP:cbp-GFP, resulting in CC fragments with a C-terminal GFP fusion. The pRAP:Rx1(45-116)-GFP3 was constructed by inserting into *Asc*I-*Nco*I–digested pRAPcbp-GFP2 the *Asc*I-*Bsp*HI fragment from pRAP:Rx1(45-116)-GFP. Rx1(45-116)-4HA was created by exchanging the GFP in pRAP:Rx1(45-116)-GFP by a 4HA tag via the *Bam*HI-*Pac*I restriction sites.

PVX CP Constructs

The PVX CP sequence was amplified from the PVX amplicons pgR106 (Jones et al., 1999) containing cDNA of the Rx1-avirulent PVX strain UK3 and pgR105 containing cDNA of the Rx1 resistance breaking strain HB (Goulden et al., 1993) using the primers 5UK3cp and 3UK3cp for cp106 and 5HBcp and 3HBcp for cp105. The products were cloned as *Bsp*HI-*Kpn*I fragments into the *Nco*I-*Kpn*I sites of pRAP. The N-terminal CFP fusions were constructed by inserting into pRAP *Asc*I-*Kpn*I the *Asc*I-*Bsp*HI 35S:CFP and the *Nco*I-*Kpn*I CP105 or CP106, resulting in pRAP:CFP-CP105 and pRAP:CFP-CP106. To provide the CP106 with NLSs in a first step, the *Bsp*HI-*Kpn*I CP fragments were cloned into pRAP:N-GFP, yielding pRAP:N-cp106. Then, this vector was opened with *Asc*I-*Spe*I followed by introduction of the *Asc*I-*Nhe*I fragment from pRAP:GFP-NLS/nls*/NES and -nes*, thereby creating pRAP:GFP-NLS-CP106, pRAP:GFP-nls-CP106, pRAP:GFP-NES-cp106, and pRAP:GFP-nes-cp106.

Rg2-ΔC-WPP-NLS

mCherry (mC) was PCR amplified from the plasmid pRSET-B mCherry (Shaner et al., 2004) with oligonucleotides mCh1 and mCh2, introducing a 5′ *Bam*HI and a 3′ *Xma*I site and subcloned in the pGEM T-easy vector, resulting in pGEM T-mCherry. For the introduction of the SV40 NLS (Haasen et al., 1999), an oligonucleotide linker was created by annealing oligonucleotides NLST1 and NLST2. The linker was ligated in *Xho*I/*Xma*I-digested pGEM T-mCherry, resulting in pGEM T-mCherry-NLS. Amplification of the RanGAP2-ΔC fragment (encoding amino acids 1 to 112 of *Nicotiana benthamiana* RanGAP2) has been described previously (Tameling and Baulcombe, 2007). This fragment was subcloned in the PCR II blunt Topo vector (Invitrogen). The fragment was cloned via *Sal*I/*Bam*HI in the binary pC/SBPc vector, of which the multiple cloning site was adapted by first ligating an oligonucleotide linker (created by annealing oligos T1 and T2) in *Xba*I/*Sal*I-digested pC/SBPc (Tameling and Baulcombe, 2007). This resulted in the Rg2-ΔC-csBP construct, in which the csBP-tag was replaced with mCherry-NLS from pGEM T-mCherry-NLS via *Bam*HI/*Xma*I to create pBIN61-Rg2-ΔC-mC-NLS.

Transient Expression

For transient expression, the expression cassettes from the pRAP constructs were cloned via *Asc*I-*Pac*I into the binary vector pBIN+ (van Engelen et al., 1995). *Agrobacterium tumefaciens* MOG101 (Hood et al., 1993) harboring the individual binary vectors was grown at 28°C in YEB medium (per liter: 5 g beef extract, 1 g yeast extract, 5 g peptone, 5 g sucrose, and 2 mL 1 M $MgSO_4$) with 50 mg/L kanamycin and 20 mg/L rifampicin. The bacteria were spun down and resuspended in MMAi infiltration medium (per liter: 5 g Murashige and Skoog salts, 1.95 g MES, 20 g sucrose, and 1 mL 200 mM acetosyringone; Sigma-Aldrich). The bacterial solution was diluted to an OD_{600} of 0.5 in MMAi and incubated at room temperature for 2 h before infiltration in *N. benthamiana* leaves. Infiltrated leaves were harvested 2 or 3 d after infiltration (depending on the expressed construct) for microscopy or protein extraction.

Confocal Microscopy and FRAP

Images of the fluorescent protein constructs in *N. benthamiana* epidermal cells were obtained using a Zeiss LSM 510 confocal microscope (Carl Zeiss) with a ×40 1.2–numerical aperture water-corrected objective. For GFP imaging, the 488-nm line from an argon laser was used for excitation, and a 505- to 550-nm band-pass filter for detection of emission. The 458-nm line of a HeNe laser and a 470- to 500-nm band-pass filter were used for CFP excitation and emission, respectively. The red fluorescent mCherry was imaged using a 543-nm HeNe laser for excitation and a 600- to 650-nm band-pass filter for emission detection. Chlorophyll emission was detected through a 650-nm long-pass filter. Fluorescence intensities were quantified using the Java application ImageJ (Abramoff et al., 2004). FRAP experiments were performed with the Zeiss LSM 510 confocal microscope. A square 12-μm^2 region in the nucleus was bleached with the 488-nm laser line at 75% power and fluorescence recovery monitored with 60-ms intervals for 5 s. Per construct, 20 to 35 recovery curves were acquired with LSM 510 software. Half-times ($\tau_{1/2}$) were determined by fitting bleaching corrected and normalized curves against a model for two-dimensional diffusion. Effective diffusion coefficients (D_{eff}, $\mu m^{-2}\ s^{-1}$) were derived from $\tau_{1/2}$ via $D_{eff} = A/(4\ \tau_{1/2})$, in which A represents the bleached surface. Statistical analyses were performed with the software package SPSS (SPSS for Windows 12.01).

Protein Extraction and Immunodetection

To extract protein from leaf samples, 0.5 g of leaf material was ground in extraction buffer (150 mM NaCl, 50 mM Tris-HCl, pH 7.5, 1 mM EDTA, 10% glycerol, 10 mM DTT, 2% polyvinylpolpyrrolidone, and 0.5 mg/mL pefabloc SC protease inhibitor [Roche]). After spinning down the cell debris (5 min, 16,000 rpm) the supernatant was combined with 4× Laemmli buffer, and the proteins were loaded on SDS-PAGE Tris-glycine or 3 to 8% Tris-Acetate gels (NuPage Novex; Invitrogen) for electrophoretic separation. SDS-PAGE separated protein was either detected with Coomassie Brilliant Blue staining or dry blotted on a nitrocellulose membrane (Immobilon-p; Millipore). GFP-fused proteins were detected on immunoblots by polyclonal rabbit anti-GFP (Abcam; 290-50) as primary antibody and peroxidase-conjugated Goat anti-Rabbit IgG (Jackson; 111-035-045) as secondary antibody. HA-tagged constructs were detected using a peroxidase-conjugated rat anti-HA antibody (Roche 10836800). The peroxidase activity was visualized with SuperSignal West

Femto and Dura luminescent substrates (Thermo Scientific, Pierce) and detected with a Syngene G:Box gel documentation system .

Plant Transformation and Virus Resistance Assay

The susceptible potato (*Solanum tuberosum*) line V was used for *Agrobacterium*-mediated plant transformation (van Engelen et al., 1994). Genomic DNA was extracted using the DNeasy plant mini kit (Qiagen) and used for PCR analysis to check the incorporation of the transgenes in the plant genome. Primary transformants were used in the virus resistance assay. To obtain infectious virus particles, leaves of *N. benthamiana* were agroinfiltrated with the PVX amplicons pGR106 and pGR105. Systemically infected leaf material was homogenized in 10 mL of 50 mM sodium phosphate buffer, pH 7, including 1 mM Pefabloc. Twenty microliters was used for sap inoculation of the four lower leaves of 4-week-old transgenic potato plants dusted with carborundum powder. Inoculations were done in triplo. Infected plants were grown in the greenhouse at 20°C and 16 h of light. Three weeks after infection, leaf discs sampled from compound leaves of the apex were homogenized as described above, and the virus concentration was determined using DAS-ELISA (Mäki-Valkama et al., 2000). Plates were coated with a 1:1000 dilution of a polyclonal antibody against PVX to bind the antigen, and a second polyclonal antibody against PVX conjugated with alkaline phosphatase was used for detection via the phosphatase substrate *p*-nitrophenyl phosphate.

Virus-Induced Gene Silencing

Three-week-old *N. benthamiana* plants were coinfiltrated with *Agrobacterium* GV3101 containing TRV1 and TRV2 vectors (Hellens et al., 2000; Ratcliff et al., 2001). The TRV silencing vector TRV2:SGT1 was kindly provided by M. Joosten (Gabriëls et al., 2006, 2007). The empty TRV2 vector was used as negative control, and TRV2:PDS (phytoene desaturase; Ratcliff et al., 2001) was used to visualize the silencing progression. Three or four weeks after inoculation, the upper leaves of the plants were used for transient expression of the fluorescent Rx1 proteins.

Accession Numbers

Sequence data from this article can be found in the GenBank/EMBL data libraries under the following accession numbers: *S. tuberosum Rx1*, AJ011801; pgR106 (PVX UK3 based vector), AY297843.1; PVX HB, X72214.1; and *N. benthamiana RanGAP2*, EF396237.

Supplemental Data

The following materials are available in the online version of this article.

Supplemental Figure 1. Activation of Endogenous Promoter Expressed Rx1 (pRXI:Rx1) by the Avirulent PVX CP (CP106) and a Fluorescent Protein Fusion Thereof (CFP-CP106).

Supplemental Figure 2. Rx1-Mediated Cell Death Is Suppressed in *SGT1*-Silenced *Nicotiana benthamiana*.

Supplemental Figure 3. Anti-GFP Immunoblot of the GFP-Fused CC Fragments.

Supplemental Figure 4. Relocalization of GFP-Rx1 in SGT1-Silenced Cells under Influence of an NLS-Fused RanGAP2 WPP Construct.

Supplemental Table 1. Nucleotide Sequences of the Oligonucleotides Used in Plasmid Construction.

ACKNOWLEDGMENTS

We thank David Baulcombe for providing the PVX amplicons pGR105 and pGR106 and Frank Takken for the critical reading of the manuscript. This research was funded by the European Union projects INSIGHT INSIDE (QLRT2000-01428) and BIOEXPLOIT (CT-2005-513959), the Dutch Technology Foundation (STW) Project 4797, and within the research program of the Centre of BioSystems Genomics, which is part of the Netherlands Genomics Initiative/Netherlands Organization for Scientific Research. L.N.S. and A.-J.P. also acknowledge Consiliul Naţional al Cercetării Ştiinţifice din Învăţământul Superior Grant PN2-ID-249 168/2007.

Received June 19, 2010; revised October 18, 2010; accepted November 19, 2010; published December 21, 2010.

REFERENCES

Aarts, N., Metz, M., Holub, E., Staskawicz, B.J., Daniels, M.J., and Parker, J.E. (1998). Different requirements for EDS1 and NDR1 by disease resistance genes define at least two R gene-mediated signaling pathways in Arabidopsis. Proc. Natl. Acad. Sci. USA **95:** 10306–10311.

Abramoff, M.D., Magalhaes, P.J., and Ram, S.J. (2004). Image processing with imageJ. Biophotonics International **11:** 36–41.

Alber, F., Dokudovskaya, S., Veenhoff, L.M., Zhang, W., Kipper, J., Devos, D., Suprapto, A., Karni-Schmidt, O., Williams, R., Chait, B. T., Sali, A., and Rout, M.P. (2007). The molecular architecture of the nuclear pore complex. Nature **450:** 695–701.

Austin, M.J., Muskett, P., Kahn, K., Feys, B.J., Jones, J.D.G., and Parker, J.E. (2002). Regulatory role of SGT1 in early R gene-mediated plant defenses. Science **295:** 2077–2080.

Azevedo, C., Betsuyaku, S., Peart, J., Takahashi, A., Noël, L., Sadanandom, A., Casais, C., Parker, J., and Shirasu, K. (2006). Role of SGT1 in resistance protein accumulation in plant immunity. EMBO J. **25:** 2007–2016.

Azevedo, C., Sadanandom, A., Kitagawa, K., Freialdenhoven, A., Shirasu, K., and Schulze-Lefert, P. (2002). The RAR1 interactor SGT1, an essential component of R gene-triggered disease resistance. Science **295:** 2073–2076.

Bamunusinghe, D., Hemenway, C.L., Nelson, R.S., Sanderfoot, A.A., Ye, C.M., Silva, M.A., Payton, M., and Verchot-Lubicz, J. (2009). Analysis of potato virus X replicase and TGBp3 subcellular locations. Virology **393:** 272–285.

Batten, J.S., Yoshinari, S., and Hemenway, C. (2003). Potato virus X: A model system for virus replication, movement and gene expression. Mol. Plant Pathol. **4:** 125–131.

Beaudouin, J., Mora-Bermúdez, F., Klee, T., Daigle, N., and Ellenberg, J. (2006). Dissecting the contribution of diffusion and interactions to the mobility of nuclear proteins. Biophys. J. **90:** 1878–1894.

Bendahmane, A., Kanyuka, K., and Baulcombe, D.C. (1999). The Rx gene from potato controls separate virus resistance and cell death responses. Plant Cell **11:** 781–792.

Bent, A.F., Kunkel, B.N., Dahlbeck, D., Brown, K.L., Schmidt, R., Giraudat, J., Leung, J., and Staskawicz, B.J. (1994). RPS2 of *Arabidopsis thaliana*: A leucine-rich repeat class of plant disease resistance genes. Science **265:** 1856–1860.

Bernoux, M., Timmers, T., Jauneau, A., Brière, C., de Wit, P.J., Marco, Y., and Deslandes, L. (2008). RD19, an *Arabidopsis* cysteine protease required for RRS1-R-mediated resistance, is relocalized to the nucleus by the *Ralstonia solanacearum* PopP2 effector. Plant Cell **20:** 2252–2264.

Bhattacharjee, S., Zamora, A., Azhar, M.T., Sacco, M.A., Lambert, L.H., and Moffett, P. (2009). Virus resistance induced by NB-LRR proteins involves Argonaute4-dependent translational control. Plant J. **58:** 940–951.

Bieri, S., Mauch, S., Shen, Q.H., Peart, J., Devoto, A., Casais, C., Ceron, F., Schulze, S., Steinbiss, H.H., Shirasu, K., and Schulze-Lefert, P. (2004). RAR1 positively controls steady state levels of barley MLA resistance proteins and enables sufficient MLA6 accumulation for effective resistance. Plant Cell **16:** 3480–3495.

Botër, M., Amigues, B., Peart, J., Breuer, C., Kadota, Y., Casais, C., Moore, G., Kleanthous, C., Ochsenbein, F., Shirasu, K., and Guerois, R. (2007). Structural and functional analysis of SGT1 reveals that its interaction with HSP90 is required for the accumulation of Rx, an R protein involved in plant immunity. Plant Cell **19:** 3791–3804.

Boyes, D.C., Nam, J., and Dangl, J.L. (1998). The *Arabidopsis thaliana* RPM1 disease resistance gene product is a peripheral plasma membrane protein that is degraded coincident with the hypersensitive response. Proc. Natl. Acad. Sci. USA **95:** 15849–15854.

Brkljacic, J., Zhao, Q., and Meier, I. (2009). WPP-domain proteins mimic the activity of the HSC70-1 chaperone in preventing mistargeting of RanGAP1-anchoring protein WIT1. Plant Physiol. **151:** 142–154.

Burch-Smith, T.M., Schiff, M., Caplan, J.L., Tsao, J., Czymmek, K., and Dinesh-Kumar, S.P. (2007). A novel role for the TIR domain in association with pathogen-derived elicitors. PLoS Biol. **5:** e68.

Caplan, J., Padmanabhan, M., and Dinesh-Kumar, S.P. (2008a). Plant NB-LRR immune receptors: From recognition to transcriptional reprogramming. Cell Host Microbe **3:** 126–135.

Caplan, J.L., Mamillapalli, P., Burch-Smith, T.M., Czymmek, K., and Dinesh-Kumar, S.P. (2008b). Chloroplastic protein NRIP1 mediates innate immune receptor recognition of a viral effector. Cell **132:** 449–462.

Carrero, G., McDonald, D., Crawford, E., de Vries, G., and Hendzel, M.J. (2003). Using FRAP and mathematical modeling to determine the in vivo kinetics of nuclear proteins. Methods **29:** 14–28.

Cazalé, A.C., Clément, M., Chiarenza, S., Roncato, M.A., Pochon, N., Creff, A., Marin, E., Leonhardt, N., and Noël, L.D. (2009). Altered expression of cytosolic/nuclear HSC70-1 molecular chaperone affects development and abiotic stress tolerance in *Arabidopsis thaliana*. J. Exp. Bot. **60:** 2653–2664.

Cheng, Y.T., Germain, H., Wiermer, M., Bi, D., Xu, F., García, A.V., Wirthmueller, L., Després, C., Parker, J.E., Zhang, Y., and Li, X. (2009). Nuclear pore complex component MOS7/Nup88 is required for innate immunity and nuclear accumulation of defense regulators in *Arabidopsis*. Plant Cell **21:** 2503–2516.

Chou, K.C. (2000). Prediction of tight turns and their types in proteins. Anal. Biochem. **286:** 1–16.

Christophe, D., Christophe-Hobertus, C., and Pichon, B. (2000). Nuclear targeting of proteins: How many different signals? Cell. Signal. **12:** 337–341.

Chuderland, D., Konson, A., and Seger, R. (2008). Identification and characterization of a general nuclear translocation signal in signaling proteins. Mol. Cell **31:** 850–861.

Cingolani, G., Bednenko, J., Gillespie, M.T., and Gerace, L. (2002). Molecular basis for the recognition of a nonclassical nuclear localization signal by importin beta. Mol. Cell **10:** 1345–1353.

Cohen, C., and Parry, D.A.D. (1986). Alpha-helical coiled coils - A widespread motif in proteins. Trends Biochem. Sci. **11:** 245–248.

Cokol, M., Nair, R., and Rost, B. (2000). Finding nuclear localization signals. EMBO Rep. **1:** 411–415.

Cole, C., Barber, J.D., and Barton, G.J. (2008). The Jpred 3 secondary structure prediction server. Nucleic Acids Res. **36** (Web Server issue): W197–W201.

Collier, S.M., and Moffett, P. (2009). NB-LRRs work a "bait and switch" on pathogens. Trends Plant Sci. **14:** 521–529.

Cook, A., Bono, F., Jinek, M., and Conti, E. (2007). Structural biology of nucleocytoplasmic transport. Annu. Rev. Biochem. **76:** 647–671.

Deslandes, L., Olivier, J., Theulieres, F., Hirsch, J., Feng, D.X., Bittner-Eddy, P., Beynon, J., and Marco, Y. (2002). Resistance to *Ralstonia solanacearum* in *Arabidopsis thaliana* is conferred by the recessive RRS1-R gene, a member of a novel family of resistance genes. Proc. Natl. Acad. Sci. USA **99:** 2404–2409.

Deslandes, L., Olivier, J., Peeters, N., Feng, D.X., Khounlotham, M., Boucher, C., Somssich, I., Genin, S., and Marco, Y. (2003). Physical interaction between RRS1-R, a protein conferring resistance to bacterial wilt, and PopP2, a type III effector targeted to the plant nucleus. Proc. Natl. Acad. Sci. USA **100:** 8024–8029.

de Wit, P.J. (2002). Plant biology: On guard. Nature **416:** 801–803.

Dodds, P.N., Lawrence, G.J., Catanzariti, A.M., Teh, T., Wang, C.I., Ayliffe, M.A., Kobe, B., and Ellis, J.G. (2006). Direct protein interaction underlies gene-for-gene specificity and coevolution of the flax resistance genes and flax rust avirulence genes. Proc. Natl. Acad. Sci. USA **103:** 8888–8893.

Dostie, J., Ferraiuolo, M., Pause, A., Adam, S.A., and Sonenberg, N. (2000). A novel shuttling protein, 4E-T, mediates the nuclear import of the mRNA 5′ cap-binding protein, eIF4E. EMBO J. **19:** 3142–3156.

Echeverría, P.C., Mazaira, G., Erlejman, A., Gomez-Sanchez, C., Piwien Pilipuk, G., and Galigniana, M.D. (2009). Nuclear import of the glucocorticoid receptor-hsp90 complex through the nuclear pore complex is mediated by its interaction with Nup62 and importin beta. Mol. Cell. Biol. **29:** 4788–4797.

Eisenberg, D., Marcotte, E.M., Xenarios, I., and Yeates, T.O. (2000). Protein function in the post-genomic era. Nature **405:** 823–826.

Enright, A.J., and Ouzounis, C.A. (2001). Functional associations of proteins in entire genomes by means of exhaustive detection of gene fusions. Genome Biol. **2:** RESEARCH0034.

Fagerlund, R., Mélen, K., Kinnunen, L., and Julkunen, I. (2002). Arginine/lysine-rich nuclear localization signals mediate interactions between dimeric STATs and importin alpha 5. J. Biol. Chem. **277:** 30072–30078.

Farnham, G., and Baulcombe, D.C. (2006). Artificial evolution extends the spectrum of viruses that are targeted by a disease-resistance gene from potato. Proc. Natl. Acad. Sci. USA **103:** 18828–18833.

Fedorkin, O.N., Solovyev, A.G., Yelina, N.E., Zamyatnin, A.A., Jr., Zinovkin, R.A., Mäkinen, K., Schiemann, J., and Yu Morozov, S. (2001). Cell-to-cell movement of potato virus X involves distinct functions of the coat protein. J. Gen. Virol. **82:** 449–458.

Feys, B.J., Moisan, L.J., Newman, M.A., and Parker, J.E. (2001). Direct interaction between the Arabidopsis disease resistance signaling proteins, EDS1 and PAD4. EMBO J. **20:** 5400–5411.

Feys, B.J., Wiermer, M., Bhat, R.A., Moisan, L.J., Medina-Escobar, N., Neu, C., Cabral, A., and Parker, J.E. (2005). Arabidopsis SENESCENCE-ASSOCIATED GENE101 stabilizes and signals within an ENHANCED DISEASE SUSCEPTIBILITY1 complex in plant innate immunity. Plant Cell **17:** 2601–2613.

Gabriëls, S.H., Takken, F.L., Vossen, J.H., de Jong, C.F., Liu, Q., Turk, S.C., Wachowski, L.K., Peters, J., Witsenboer, H.M., de Wit, P.J., and Joosten, M.H. (2006). CDNA-AFLP combined with functional analysis reveals novel genes involved in the hypersensitive response. Mol. Plant Microbe Interact. **19:** 567–576.

Gabriëls, S.H., Vossen, J.H., Ekengren, S.K., van Ooijen, G., Abd-El-Haliem, A.M., van den Berg, G.C., Rainey, D.Y., Martin, G.B., Takken, F.L., de Wit, P.J., and Joosten, M.H. (2007). An NB-LRR protein required for HR signalling mediated by both extra- and intracellular resistance proteins. Plant J. **50:** 14–28.

Gallant, P. (2007). Control of transcription by Pontin and Reptin. Trends Cell Biol. **17:** 187–192.

García, A.V., Blanvillain-Baufumé, S., Huibers, R.P., Wiermer, M., Li, G., Gobbato, E., Rietz, S., and Parker, J.E. (2010). Balanced nuclear and cytoplasmic activities of EDS1 are required for a complete plant innate immune response. PLoS Pathog. **6:** e1000970.

Garnier, J., Gibrat, J.F., and Robson, B. (1996). GOR method for predicting protein secondary structure from amino acid sequence. Methods Enzymol. **266:** 540–553.

Geer, L.Y., Domrachev, M., Lipman, D.J., and Bryant, S.H. (2002). CDART: Protein homology by domain architecture. Genome Res. **12:** 1619–1623.

Geourjon, C., and Deléage, G. (1995). SOPMA: Significant improvements in protein secondary structure prediction by consensus prediction from multiple alignments. Comput. Appl. Biosci. **11:** 681–684.

Görisch, S.M., Wachsmuth, M., Tóth, K.F., Lichter, P., and Rippe, K. (2005). Histone acetylation increases chromatin accessibility. J. Cell Sci. **118:** 5825–5834.

Görlich, D., and Kutay, U. (1999). Transport between the cell nucleus and the cytoplasm. Annu. Rev. Cell Dev. Biol. **15:** 607–660.

Görlich, D., Panté, N., Kutay, U., Aebi, U., and Bischoff, F.R. (1996). Identification of different roles for RanGDP and RanGTP in nuclear protein import. EMBO J. **15:** 5584–5594.

Gorski, S.A., Dundr, M., and Misteli, T. (2006). The road much traveled: trafficking in the cell nucleus. Curr. Opin. Cell Biol. **18:** 284–290.

Goulden, M.G., Köhm, B.A., Santa Cruz, S., Kavanagh, T.A., and Baulcombe, D.C. (1993). A feature of the coat protein of potato virus X affects both induced virus resistance in potato and viral fitness. Virology **197:** 293–302.

Grant, M.R., Godiard, L., Straube, E., Ashfield, T., Lewald, J., Sattler, A., Innes, R.W., and Dangl, J.L. (1995). Structure of the Arabidopsis RPM1 gene enabling dual specificity disease resistance. Science **269:** 843–846.

Guermeur, Y. (1997). Combinaison de classifieurs statistiques, Application à la prédiction de la structure secondaire des protéines. In Laboratoire d'Informatique, V. Mangin, ed (Paris: Université Paris 6), pp. 164.

Haasen, D., Köhler, C., Neuhaus, G., and Merkle, T. (1999). Nuclear export of proteins in plants: AtXPO1 is the export receptor for leucine-rich nuclear export signals in *Arabidopsis thaliana*. Plant J. **20:** 695–705.

Hager, G.L., McNally, J.G., and Misteli, T. (2009). Transcription dynamics. Mol. Cell **35:** 741–753.

Heese, A., Hann, D.R., Gimenez-Ibanez, S., Jones, A.M., He, K., Li, J., Schroeder, J.I., Peck, S.C., and Rathjen, J.P. (2007). The receptor-like kinase SERK3/BAK1 is a central regulator of innate immunity in plants. Proc. Natl. Acad. Sci. USA **104:** 12217–12222.

Hellens, R.P., Edwards, E.A., Leyland, N.R., Bean, S., and Mullineaux, P.M. (2000). pGreen: a versatile and flexible binary Ti vector for Agrobacterium-mediated plant transformation. Plant Mol. Biol. **42:** 819–832.

Holt, B.F., 3rd, Belkhadir, Y., and Dangl, J.L. (2005). Antagonistic control of disease resistance protein stability in the plant immune system. Science **309:** 929–932.

Holt, B.F., 3rd, Boyes, D.C., Ellerström, M., Siefers, N., Wiig, A., Kauffman, S., Grant, M.R., and Dangl, J.L. (2002). An evolutionarily conserved mediator of plant disease resistance gene function is required for normal Arabidopsis development. Dev. Cell **2:** 807–817.

Hood, E.E., Gelvin, S.B., Melchers, L.S., and Hoekema, A. (1993). New *Agrobacterium* helper plasmids for gene transfer to plants. Transgenic Res. **2:** 208–218.

Houtsmuller, A.B. (2005). Fluorescence recovery after photobleaching: Application to nuclear proteins. In Microscopy Techniques, J. Rietdorf, ed (Berlin/Heidelberg: Springer), pp. 177–199.

Hutten, S., and Kehlenbach, R.H. (2007). CRM1-mediated nuclear export: to the pore and beyond. Trends Cell Biol. **17:** 193–201.

Jeong, S.Y., Rose, A., Joseph, J., Dasso, M., and Meier, I. (2005). Plant-specific mitotic targeting of RanGAP requires a functional WPP domain. Plant J. **42:** 270–282.

Jia, Y., McAdams, S.A., Bryan, G.T., Hershey, H.P., and Valent, B. (2000). Direct interaction of resistance gene and avirulence gene products confers rice blast resistance. EMBO J. **19:** 4004–4014.

Jones, D.A., and Takemoto, D. (2004). Plant innate immunity - Direct and indirect recognition of general and specific pathogen-associated molecules. Curr. Opin. Immunol. **16:** 48–62.

Jones, D.T. (1999). Protein secondary structure prediction based on position-specific scoring matrices. J. Mol. Biol. **292:** 195–202.

Jones, J.D., and Dangl, J.L. (2006). The plant immune system. Nature **444:** 323–329.

Jones, L., Hamilton, A.J., Voinnet, O., Thomas, C.L., Maule, A.J., and Baulcombe, D.C. (1999). RNA-DNA interactions and DNA methylation in post-transcriptional gene silencing. Plant Cell **11:** 2291–2301.

Kang, K.I., Devin, J., Cadepond, F., Jibard, N., Guiochon-Mantel, A., Baulieu, E.E., and Catelli, M.G. (1994). In vivo functional protein-protein interaction: Nuclear targeted hsp90 shifts cytoplasmic steroid receptor mutants into the nucleus. Proc. Natl. Acad. Sci. USA **91:** 340–344.

Karpova, O.V., Zayakina, O.V., Arkhipenko, M.V., Sheval, E.V., Kiselyova, O.I., Poljakov, V.Y., Yaminsky, I.V., Rodionova, N.P., and Atabekov, J.G. (2006). Potato virus X RNA-mediated assembly of single-tailed ternary 'coat protein-RNA-movement protein' complexes. J. Gen. Virol. **87:** 2731–2740.

Kobe, B., and Kajava, A.V. (2001). The leucine-rich repeat as a protein recognition motif. Curr. Opin. Struct. Biol. **11:** 725–732.

Kohler, A., Rinaldi, C., Duplessis, S., Baucher, M., Geelen, D., Duchaussoy, F., Meyers, B.C., Boerjan, W., and Martin, F. (2008). Genome-wide identification of NBS resistance genes in *Populus trichocarpa*. Plant Mol. Biol. **66:** 619–636.

Kose, S., Furuta, M., Koike, M., Yoneda, Y., and Imamoto, N. (2005). The 70-kD heat shock cognate protein (hsc70) facilitates the nuclear export of the import receptors. J. Cell Biol. **171:** 19–25.

Kozak, M. (1995). Adherence to the first-AUG rule when a second AUG codon follows closely upon the first. Proc. Natl. Acad. Sci. USA **92:** 7134.

Kozak, M. (1999). Initiation of translation in prokaryotes and eukaryotes. Gene **234:** 187–208.

la Cour, T., Kiemer, L., Mølgaard, A., Gupta, R., Skriver, K., and Brunak, S. (2004). Analysis and prediction of leucine-rich nuclear export signals. Protein Eng. Des. Sel. **17:** 527–536.

Lahaye, T. (2002). The Arabidopsis RRS1-R disease resistance gene—Uncovering the plant's nucleus as the new battlefield of plant defense? Trends Plant Sci. **7:** 425–427.

Lanford, R.E., and Butel, J.S. (1984). Construction and characterization of an SV40 mutant defective in nuclear transport of T antigen. Cell **37:** 801–813.

Lange, A., Mills, R.E., Devine, S.E., and Corbett, A.H. (2008). A PY-NLS nuclear targeting signal is required for nuclear localization and function of the *Saccharomyces cerevisiae* mRNA-binding protein Hrp1. J. Biol. Chem. **283:** 12926–12934.

Lange, A., Mills, R.E., Lange, C.J., Stewart, M., Devine, S.E., and Corbett, A.H. (2007). Classical nuclear localization signals: Definition, function, and interaction with importin alpha. J. Biol. Chem. **282:** 5101–5105.

Launholt, D., Merkle, T., Houben, A., Schulz, A., and Grasser, K.D. (2006). Arabidopsis chromatin-associated HMGA and HMGB use different nuclear targeting signals and display highly dynamic localization within the nucleus. Plant Cell **18:** 2904–2918.

Lee, B.J., Cansizoglu, A.E., Süel, K.E., Louis, T.H., Zhang, Z., and Chook, Y.M. (2006). Rules for nuclear localization sequence recognition by karyopherin beta 2. Cell **126:** 543–558.

Leister, R.T., Dahlbeck, D., Day, B., Li, Y., Chesnokova, O., and Staskawicz, B.J. (2005). Molecular genetic evidence for the role of

SGT1 in the intramolecular complementation of Bs2 protein activity in *Nicotiana benthamiana*. Plant Cell **17:** 1268–1278.

Linding, R., Jensen, L.J., Diella, F., Bork, P., Gibson, T.J., and Russell, R.B. (2003). Protein disorder prediction: Implications for structural proteomics. Structure **11:** 1453–1459.

Liu, Y., Burch-Smith, T., Schiff, M., Feng, S., and Dinesh-Kumar, S.P. (2004). Molecular chaperone Hsp90 associates with resistance protein N and its signaling proteins SGT1 and Rar1 to modulate an innate immune response in plants. J. Biol. Chem. **279:** 2101–2108.

Lu, R., Malcuit, I., Moffett, P., Ruiz, M.T., Peart, J., Wu, A.J., Rathjen, J.P., Bendahmane, A., Day, L., and Baulcombe, D.C. (2003). High throughput virus-induced gene silencing implicates heat shock protein 90 in plant disease resistance. EMBO J. **22:** 5690–5699.

Lupas, A. (1997). Predicting coiled-coil regions in proteins. Curr. Opin. Struct. Biol. **7:** 388–393.

Mäki-Valkama, T., Valkonen, J.P., Kreuze, J.F., and Pehu, E. (2000). Transgenic resistance to PVY(O) associated with post-transcriptional silencing of P1 transgene is overcome by PVY(N) strains that carry highly homologous P1 sequences and recover transgene expression at infection. Mol. Plant Microbe Interact. **13:** 366–373.

Martin, G.B., Bogdanove, A.J., and Sessa, G. (2003). Understanding the functions of plant disease resistance proteins. Annu. Rev. Plant Biol. **54:** 23–61.

McNally, J.G. (2008). Quantitative FRAP in analysis of molecular binding dynamics in vivo. In Methods in Cell Biology, K.F. Sullivan, ed (San Diego: Academic Press), pp. 329–351.

Merkle, T. (2003). Nucleo-cytoplasmic partitioning of proteins in plants: Implications for the regulation of environmental and developmental signalling. Curr. Genet. **44:** 231–260.

Miyazaki, S., Kuroda, Y., and Yokoyama, S. (2002). Characterization and prediction of linker sequences of multi-domain proteins by a neural network. J. Struct. Funct. Genomics **2:** 37–51.

Moffett, P., Farnham, G., Peart, J., and Baulcombe, D.C. (2002). Interaction between domains of a plant NBS-LRR protein in disease resistance-related cell death. EMBO J. **21:** 4511–4519.

Mohr, D., Frey, S., Fischer, T., Güttler, T., and Görlich, D. (2009). Characterisation of the passive permeability barrier of nuclear pore complexes. EMBO J. **28:** 2541–2553.

Mueller, F., Mazza, D., Stasevich, T.J., and McNally, J.G. (2010). FRAP and kinetic modeling in the analysis of nuclear protein dynamics: What do we really know? Curr. Opin. Cell Biol. **22:** 403–411.

Narusaka, M., Shirasu, K., Noutoshi, Y., Kubo, Y., Shiraishi, T., Iwabuchi, M., and Narusaka, Y. (2009). RRS1 and RPS4 provide a dual Resistance-gene system against fungal and bacterial pathogens. Plant J. **60:** 218–226.

Navarro, L., Zipfel, C., Rowland, O., Keller, I., Robatzek, S., Boller, T., and Jones, J.D. (2004). The transcriptional innate immune response to flg22. Interplay and overlap with Avr gene-dependent defense responses and bacterial pathogenesis. Plant Physiol. **135:** 1113–1128.

Noël, L.D., Cagna, G., Stuttmann, J., Wirthmüller, L., Betsuyaku, S., Witte, C.P., Bhat, R., Pochon, N., Colby, T., and Parker, J.E. (2007). Interaction between SGT1 and cytosolic/nuclear HSC70 chaperones regulates *Arabidopsis* immune responses. Plant Cell **19:** 4061–4076.

Oparka, K.J., Roberts, A.G., Roberts, I.M., Prior, D.A.M., and Santa Cruz, S. (1996). Viral coat protein is targeted to, but does not gate, plasmodesmata during cell-to-cell movement of potato virus X. Plant J. **10:** 805–813.

Ouali, M., and King, R.D. (2000). Cascaded multiple classifiers for secondary structure prediction. Protein Sci. **9:** 1162–1176.

Paine, P.L., Moore, L.C., and Horowitz, S.B. (1975). Nuclear envelope permeability. Nature **254:** 109–114.

Pay, A., Resch, K., Frohnmeyer, H., Fejes, E., Nagy, F., and Nick, P. (2002). Plant RanGAPs are localized at the nuclear envelope in interphase and associated with microtubules in mitotic cells. Plant J. **30:** 699–709.

Peart, J.R., Cook, G., Feys, B.J., Parker, J.E., and Baulcombe, D.C. (2002a). An EDS1 orthologue is required for N-mediated resistance against tobacco mosaic virus. Plant J. **29:** 569–579.

Peart, J.R., et al. (2002b). Ubiquitin ligase-associated protein SGT1 is required for host and nonhost disease resistance in plants. Proc. Natl. Acad. Sci. USA **99:** 10865–10869.

Phair, R.D., Scaffidi, P., Elbi, C., Vecerová, J., Dey, A., Ozato, K., Brown, D.T., Hager, G., Bustin, M., and Misteli, T. (2004). Global nature of dynamic protein-chromatin interactions in vivo: Three-dimensional genome scanning and dynamic interaction networks of chromatin proteins. Mol. Cell. Biol. **24:** 6393–6402.

Querci, M., Baulcombe, D.C., Goldbach, R.W., and Salazar, L.F. (1995). Analysis of the resistance-breaking determinants of Potato virus X (PVX) strain Hb on different potato genotypes expressing extreme resistance to PVX. Phytopathology **85:** 1003–1010.

Quevillon, E., Silventoinen, V., Pillai, S., Harte, N., Mulder, N., Apweiler, R., and Lopez, R. (2005). InterProScan: protein domains identifier. Nucleic Acids Res. **33** (Web Server issue): W116–W120.

Rairdan, G.J., Collier, S.M., Sacco, M.A., Baldwin, T.T., Boettrich, T., and Moffett, P. (2008). The coiled-coil and nucleotide binding domains of the Potato Rx disease resistance protein function in pathogen recognition and signaling. Plant Cell **20:** 739–751.

Rairdan, G.J., and Moffett, P. (2006). Distinct domains in the ARC region of the potato resistance protein Rx mediate LRR binding and inhibition of activation. Plant Cell **18:** 2082–2093.

Ratcliff, F., Martin-Hernandez, A.M., and Baulcombe, D.C. (2001). Technical Advance. Tobacco rattle virus as a vector for analysis of gene function by silencing. Plant J. **25:** 237–245.

Reits, E.A., and Neefjes, J.J. (2001). From fixed to FRAP: Measuring protein mobility and activity in living cells. Nat. Cell Biol. **3:** E145–E147.

Rose, A., and Meier, I. (2001). A domain unique to plant RanGAP is responsible for its targeting to the plant nuclear rim. Proc. Natl. Acad. Sci. USA **98:** 15377–15382.

Sacco, M.A., Koropacka, K., Grenier, E., Jaubert, M.J., Blanchard, A., Goverse, A., Smant, G., and Moffett, P. (2009). The cyst nematode SPRYSEC protein RBP-1 elicits Gpa2- and RanGAP2-dependent plant cell death. PLoS Pathog. **5:** e1000564.

Sacco, M.A., Mansoor, S., and Moffett, P. (2007). A RanGAP protein physically interacts with the NB-LRR protein Rx, and is required for Rx-mediated viral resistance. Plant J. **52:** 82–93.

Santa Cruz, S., Chapman, S., Roberts, A.G., Roberts, I.M., Prior, D. A.M., and Oparka, K.J. (1996). Assembly and movement of a plant virus carrying a green fluorescent protein overcoat. Proc. Natl. Acad. Sci. USA **93:** 6286–6290.

Schouten, A., Roosien, J., de Boer, J.M., Wilmink, A., Rosso, M.N., Bosch, D., Stiekema, W.J., Gommers, F.J., Bakker, J., and Schots, A. (1997). Improving scFv antibody expression levels in the plant cytosol. FEBS Lett. **415:** 235–241.

Seksek, O., Biwersi, J., and Verkman, A.S. (1997). Translational diffusion of macromolecule-sized solutes in cytoplasm and nucleus. J. Cell Biol. **138:** 131–142.

Shaner, N.C., Campbell, R.E., Steinbach, P.A., Giepmans, B.N.G., Palmer, A.E., and Tsien, R.Y. (2004). Improved monomeric red, orange and yellow fluorescent proteins derived from Discosoma sp. red fluorescent protein. Nat. Biotechnol. **22:** 1567–1572.

Shen, Q.H., Saijo, Y., Mauch, S., Biskup, C., Bieri, S., Keller, B., Seki, H., Ulker, B., Somssich, I.E., and Schulze-Lefert, P. (2007). Nuclear activity of MLA immune receptors links isolate-specific and basal disease-resistance responses. Science **315:** 1098–1103.

Shen, Q.H., and Schulze-Lefert, P. (2007). Rumble in the nuclear jungle: compartmentalization, trafficking, and nuclear action of plant immune receptors. EMBO J. **26:** 4293–4301.

Shirasu, K. (2009). The HSP90-SGT1 chaperone complex for NLR immune sensors. Annu. Rev. Plant Biol. **60:** 139–164.

Sprague, B.L., and McNally, J.G. (2005). FRAP analysis of binding: Proper and fitting. Trends Cell Biol. **15:** 84–91.

Sprague, B.L., Pego, R.L., Stavreva, D.A., and McNally, J.G. (2004). Analysis of binding reactions by fluorescence recovery after photobleaching. Biophys. J. **86:** 3473–3495.

Stewart, M. (2006). Structural basis for the nuclear protein import cycle. Biochem. Soc. Trans. **34:** 701–704.

Swiderski, M.R., Birker, D., and Jones, J.D. (2009). The TIR domain of TIR-NB-LRR resistance proteins is a signaling domain involved in cell death induction. Mol. Plant Microbe Interact. **22:** 157–165.

Tago, K., Tsukahara, F., Naruse, M., Yoshioka, T., and Takano, K. (2004). Regulation of nuclear retention of glucocorticoid receptor by nuclear Hsp90. Mol. Cell. Endocrinol. **213:** 131–138.

Takahashi, A., Casais, C., Ichimura, K., and Shirasu, K. (2003). HSP90 interacts with RAR1 and SGT1 and is essential for RPS2-mediated disease resistance in Arabidopsis. Proc. Natl. Acad. Sci. USA **100:** 11777–11782.

Takken, F.L.W., Albrecht, M., and Tameling, W.I.L. (2006). Resistance proteins: Molecular switches of plant defence. Curr. Opin. Plant Biol. **9:** 383–390.

Takken, F.L.W., and Tameling, W.I.L. (2009). To nibble at plant resistance proteins. Science **324:** 744–746.

Tameling, W.I.L., and Baulcombe, D.C. (2007). Physical association of the NB-LRR resistance protein Rx with a Ran GTPase-activating protein is required for extreme resistance to Potato virus X. Plant Cell **19:** 1682–1694.

Tameling, W.I.L., Elzinga, S.D.J., Darmin, P.S., Vossen, J.H., Takken, F.L.W., Haring, M.A., and Cornelissen, B.J.C. (2002). The tomato R gene products I-2 and MI-1 are functional ATP binding proteins with ATPase activity. Plant Cell **14:** 2929–2939.

Tameling, W.I.L., Nooijen, C., Ludwig, N., Botër, M., Slootweg, E., Goverse, A., Shirasu, K., and Joosten, M.H.A.J. (2010). RanGAP2 mediates nucleo-cytoplasmic partitioning of the NB-LRR immune receptor Rx, thereby dictating Rx function. Plant Cell **22:** 4176–4194.

Tameling, W.I.L., Vossen, J.H., Albrecht, M., Lengauer, T., Berden, J.A., Haring, M.A., Cornelissen, B.J.C., and Takken, F.L.W. (2006). Mutations in the NB-ARC domain of I-2 that impair ATP hydrolysis cause autoactivation. Plant Physiol. **140:** 1233–1245.

Thompson, N.L., Lieto, A.M., and Allen, N.W. (2002). Recent advances in fluorescence correlation spectroscopy. Curr. Opin. Struct. Biol. **12:** 634–641.

Tuskan, G.A., et al. (2006). The genome of black cottonwood, *Populus trichocarpa* (Torr. & Gray). Science **313:** 1596–1604.

Ursula Stochaj, K.L.R. (1999). Nucleocytoplasmic trafficking of proteins: With or without Ran? Bioessays **21:** 579–589.

van der Vossen, E.A.G., van der Voort, J.N., Kanyuka, K., Bendahmane, A., Sandbrink, H., Baulcombe, D.C., Bakker, J., Stiekema, W.J., and Klein-Lankhorst, R.M. (2000). Homologues of a single resistance-gene cluster in potato confer resistance to distinct pathogens: A virus and a nematode. Plant J. **23:** 567–576.

van Engelen, F.A., Molthoff, J.W., Conner, A.J., Nap, J.P., Pereira, A., and Stiekema, W.J. (1995). pBINPLUS: An improved plant transformation vector based on pBIN19. Transgenic Res. **4:** 288–290.

van Engelen, F.A., Schouten, A., Molthoff, J.W., Roosien, J., Salinas, J., Dirkse, W.G., Schots, A., Bakker, J., Gommers, F.J., Jongsma, M.A., Bosch, D., and Stiekema, W.J. (1994). Coordinate expression of antibody subunit genes yields high levels of functional antibodies in roots of transgenic tobacco. Plant Mol. Biol. **26:** 1701–1710.

Wang, W., Devoto, A., Turner, J.G., and Xiao, S. (2007). Expression of the membrane-associated resistance protein RPW8 enhances basal defense against biotrophic pathogens. Mol. Plant Microbe Interact. **20:** 966–976.

Weaver, M.L., Swiderski, M.R., Li, Y., and Jones, J.D.G. (2006). The *Arabidopsis thaliana* TIR-NB-LRR R-protein, RPP1A; protein localization and constitutive activation of defence by truncated alleles in tobacco and Arabidopsis. Plant J. **47:** 829–840.

Wen, W., Meinkoth, J.L., Tsien, R.Y., and Taylor, S.S. (1995). Identification of a signal for rapid export of proteins from the nucleus. Cell **82:** 463–473.

Wirthmueller, L., Zhang, Y., Jones, J.D., and Parker, J.E. (2007). Nuclear accumulation of the Arabidopsis immune receptor RPS4 is necessary for triggering EDS1-dependent defense. Curr. Biol. **17:** 2023–2029.

Xu, L., and Massagué, J. (2004). Nucleocytoplasmic shuttling of signal transducers. Nat. Rev. Mol. Cell Biol. **5:** 209–219.

Yang, T.T., Cheng, L., and Kain, S.R. (1996). Optimized codon usage and chromophore mutations provide enhanced sensitivity with the green fluorescent protein. Nucleic Acids Res. **24:** 4592–4593.

Zipfel, C., Robatzek, S., Navarro, L., Oakeley, E.J., Jones, J.D., Felix, G., and Boller, T. (2004). Bacterial disease resistance in Arabidopsis through flagellin perception. Nature **428:** 764–767.